doi.org/10.26434/chemrxiv.7087538.v1

A New Approach to Enhancing the CO2 Capture Performance of Defective UiO-66 via Post-Synthetic Defect Exchange

Athanasios Koutsianos, Ewa Kazimierska, Andrew R. Barron, Marco Taddei, Enrico Andreoli

Submitted date: 25/09/2018 • Posted date: 26/09/2018

Citation information: Koutsianos, Athanasios; Kazimierska, Ewa; Barron, Andrew R.; Taddei, Marco; Andreoli, Enrico (2018): A New Approach to Enhancing the CO2 Capture Performance of Defective UiO-66 via Post-Synthetic Defect Exchange. ChemRxiv. Preprint.

Zirconium-based metal-organic frameworks (Zr-MOFs) are a subclass of MOFs known for their remarkable stability, especially in the presence of water. This makes them extremely attractive for practical applications, including CO_2 capture from industrial emission sources; however, the CO_2 adsorption capacity of Zr-MOFs is moderate compared to that of the best performing MOFs reported to date. Functionalization of Zr-MOFs with amino groups has been demonstrated to increase their affinity for CO_2. In this work, we assessed the potential of post-synthetic defect exchange (PSDE) as an alternative approach to introduce amino functionalities at missing-cluster defective sites in formic acid modulated UiO-66. Both pyridine-containing (picolinic acid and nicotinic acid) and aniline-containing (3-aminobenzoic acid and anthranilic acid) monocarboxylates were integrated within defective UiO-66 with this method. Non-defective UiO-66 modified with linkers bearing the same amino groups (2,5-pyridinedicarboxylic acid and 2-aminoterephthalic acid) were prepared by classical post-synthetic ligand exchange (PSE), in order to compare the effect of introducing functionalities at defective sites versus installing them on the backbone. PSDE reduces the porosity of defective UiO-66, but improves both the CO_2 uptake and the CO_2/N_2 selectivity, whereas PSE has no effect on the porosity of non-defective UiO-66, improving the CO_2 uptake but leaving selectivity unchanged. Modification of defective UiO-66 with benzoic acid reveals that pore size reduction is the main factor responsible for the observed uptake improvement, whereas the presence of nitrogen atoms in the pores seems to be beneficial for increasing selectivity.

File list (2)

Manuscript_Koutsianos.pdf (1.38 MiB)	view on ChemRxiv • download file
SI_Koutsianos.pdf (3.06 MiB)	view on ChemRxiv • download file

A new approach to enhancing the CO_2 capture performance of defective UiO-66 via post-synthetic defect exchange

Athanasios Koutsianos,[1] Ewa Kazimierska,[1] Andrew R. Barron,[1,2,3] Marco Taddei, [1] and Enrico Andreoli[1]**

[1] Energy Safety Research Institute, Swansea University, Fabian Way, Swansea, SA1 8EN, UK

[2] Department of Chemistry, Rice University, Houston, Texas, 77005, USA

[3] Department of Materials Science and Nanoengineering, Rice University, Houston, Texas, 77005, USA

ABSTRACT

Zirconium-based metal-organic frameworks (Zr-MOFs) are a subclass of MOFs known for their remarkable stability, especially in the presence of water. This makes them extremely attractive for practical applications, including CO_2 capture from industrial emission sources; however, the CO_2 adsorption capacity of Zr-MOFs is moderate compared to that of the best performing MOFs reported to date. Functionalization of Zr-MOFs with amino groups has been demonstrated to increase their affinity for CO_2. In this work, we assessed the potential of post-synthetic defect exchange (PSDE) as an alternative approach to introduce amino functionalities at missing-cluster

defective sites in formic acid modulated UiO-66. Both pyridine-containing (picolinic acid and nicotinic acid) and aniline-containing (3-aminobenzoic acid and anthranilic acid) monocarboxylates were integrated within defective UiO-66 with this method. Non-defective UiO-66 modified with linkers bearing the same amino groups (2,5-pyridinedicarboxylic acid and 2-aminoterephthalic acid) were prepared by classical post-synthetic ligand exchange (PSE), in order to compare the effect of introducing functionalities at defective sites versus installing them on the backbone. PSDE reduces the porosity of defective UiO-66, but improves both the CO_2 uptake and the CO_2/N_2 selectivity, whereas PSE has no effect on the porosity of non-defective UiO-66, improving the CO_2 uptake but leaving selectivity unchanged. Modification of defective UiO-66 with benzoic acid reveals that pore size reduction is the main factor responsible for the observed uptake improvement, whereas the presence of nitrogen atoms in the pores seems to be beneficial for increasing selectivity.

Introduction

The Committee on Climate Change (CCC) has recently released its annual report on greenhouse gases reduction progress for 2018.[1] Among the key messages of the report is the necessity to cut CO_2 emissions from industry. In contrast to the power sector, industrial emissions rose by 1% in 2017 rendering the implementation of industrial carbon capture, utilization and storage (CCUS) imperative.[1] During the last decades, post combustion capture (PCC) using liquid amines (i.e., amine scrubbing) has been used on commercial scale and it is considered to have a technology readiness level of 9.[2] According to a recent study though, PCC displays higher operation and maintenance costs than oxy-fuel and pre-combustion capture technologies.[3] The high costs are ascribed to several issues that liquid phase chemical absorption suffers from, such as equipment corrosion, high regeneration energy, solvent loss and toxicity.[4] Physical binding of CO_2 by solid

porous adsorbents has thus been proposed as an alternative for CCUS applications.[5] In this context, metal-organic frameworks (MOFs) have drawn interest as promising sorbents, owing to their high porosity and structural and chemical versatility.[6] The main pitfall that so far has hindered large scale deployment of MOFs for CCS is their limited stability in working conditions.[7]

Zr-based MOFs (Zr-MOFs) have lately become one intensely investigated subclass of MOFs, due to their remarkable stability, especially in the presence of water. This feature makes them attractive for application in industrially relevant settings, including CO_2 capture, where the presence of water is unavoidable.[8] Unfortunately, the uptake performance of Zr-MOFs appears moderate, when compared with other MOFs,[7] and they suffer from low selectivity, a necessary feature for separation of dilute CO_2 streams in the low partial pressures regime.[9] Chemical modification of MOFs with nitrogen atoms has been investigated, aiming at a more polar sorption material and the resulting enhanced dipole-quadrupole interactions between CO_2 molecules and the nitrogen sites of the sorbent.[9] Framework functionalization via direct synthesis using either linkers bearing amino functionalities or nitrogen containing heterocycles have been used and afforded enhanced affinity for CO_2 in Zr-MOFs.[10-12] This enhancement was attributed to either (a) cooperation between -NH_2 groups and -OH groups in the clusters in binding CO_2 molecules[10] or (b) presence of nucleophilic heterocyclic nitrogen species.[12] A similar trend was also displayed by Zr-MOFs where ethanolamine was post-synthetically grafted to the clusters, which led to efficient CO_2 capture by formation of carbamate species.[13]

The presence of structural defects in Zr-MOFs has been recently revealed and the subsequent exploitation of defects towards tuning of physical-chemical properties has drawn considerable attention.[14-17] With regard to CO_2 capture, a recent study demonstrated that

monocarboxylate groups derived from crystallization modulators and grafted at the missing-cluster defective sites in the prototypical Zr-MOF UiO-66, based on 1,4-benzenedicarboxylic acid (terephthalic acid, BDC) and having ideal formula $Zr_6O_4OH_4(BDC)_6$, can be post-synthetically exchanged with *L*-serine ligands, enhancing capture capacity.[18] We recently observed that when soaked in a solution of a terephthalic acid analogue, defective UiO-66 undergoes preferential exchange of defect-compensating monocarboxylic groups rather than replacement of linker molecules constituting the framework backbone.[19] This process is termed post-synthetic defect exchange (PSDE). The textural and CO_2 sorption properties of the resulting MOFs were influenced in a different manner to when the terephthalic acid analogue was installed in the framework. These results prompted us to systematically investigate the potential of PSDE as a method for improving the CO_2 capture performance of defective UiO-66. The goal of this study was to incorporate a range of monocarboxylate species bearing nitrogen moieties within UiO-66 via PSDE, with the aim of tailoring the physical-chemical properties of the sorbent material and examine if and how the nature and orientation of the amino functional groups affect the sorption properties. Dicarboxylic linker analogues were introduced in non-defective UiO-66 by classical post-synthetic ligand exchange (PSE), in order to compare the different effects of defect functionalization and framework functionalization on the physical-chemical properties.

Experimental Section

Chemicals

$ZrCl_4$ (98%) and 2-amino-1,4-benzenedicarboxylic acid (ABDC, 99%) were purchased from Acros Organics. 1,4-benzenedicarboxylic acid (BDC, 98%) and benzoic acid (BA, 99%) were purchased from Alfa Aesar. Formic acid (FA, 98-100%), 2,5-pyridinedicarboxylic acid (PyDC)

and anthranilic acid (AA, 99%) were purchased from Merck Millipore. *N*,*N*-dimethylformamide (DMF) was purchased from VWR. Nicotinic acid (NA, 99%) was provided by Sigma. 3-aminobenzoic acid and picolinic acid (PA, 99%) were purchased from Aldrich. Chemical structures of chemicals are provided in Figure 1.

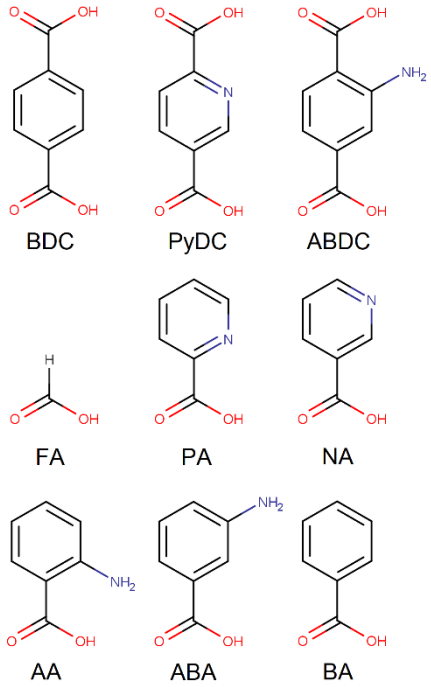

Figure 1. Chemical structures of the carboxylic acids employed in this study: terephthalic acid (BDC), 2,5-pyridinedicarboxylic acid (PyDC), 2-aminoterephthalic acid (ABDC), formic acid (FA), picolinic acid (PA), nicotinic acid (NA), 3-aminobenzoic acid (ABA), anthranilic acid (AA) and benzoic acid (BA).

Synthetic procedures

Synthesis of FA_mod

$ZrCl_4$ (1.165 g, 5.000 mmol) was dissolved in DMF (81 mL), followed by the addition of water (0.270 mL, 15.0 mmol), FA (18.8 mL, 500 mmol) and BDC (0.870 g, 5.00 mmol). The mixture

was sonicated until complete dissolution, divided into ten 20 mL vials and kept for 16 hours at 120 °C. The solid was subsequently centrifuged and washed with DMF (25 mL, one-hour soaking), water (2 × 25 mL, one-hour soaking) and acetone (25 mL, one-hour soaking; 25 mL, overnight soaking). The solid was dried in air at 80 °C for two hours.

Synthesis of defect-engineered materials

FA_mod-NA, FA_mod-PA, FA_mod-BA, FA_mod-ABA and FA_mod-AA resulted from the suspension of FA_mod (500 mg) in the respective solution of NA, PA, BA, ABA and AA (0.025 M) in DMF (33 mL) for 24 hours at 80 °C. Afterwards the solids were centrifuged and washed with DMF (25 mL, one-hour soaking), water (2 × 25 mL, one-hour soaking) and acetone (25 mL, one-hour soaking; 25 mL, overnight soaking). The solids were dried in air at 80 °C for two hours.

Synthesis of No_mod

$ZrCl_4$ (1.165 g, 5.000 mmol) was dissolved in DMF (100 mL), followed by the addition of water (0.270 mL, 15.0 mmol) and BDC (0.870 g, 5.00 mmol). The mixture was sonicated until complete dissolution, divided into ten 20 mL vials and kept for 16 hours at 120 °C. The solid was subsequently centrifuged and washed with DMF (25 mL, one-hour soaking), water (2 × 25 mL, two-hour soaking) and acetone (25 mL, one-hour soaking; 25 mL, overnight soaking). The solid was dried in air at 80 °C for two hours.

Synthesis of No_mod-PyDC

No_mod (500 mg) was suspended in a solution of PyDC (0.025 M) in DMF (33 mL) for 24 hours at 80 °C. The solid was then centrifuged and washed with DMF (25 mL, one-hour

soaking), water (2 × 25 mL, two-hour soaking) and acetone (25 mL, one-hour soaking; 25 mL, overnight soaking). The solid was dried in air at 80 °C for two hours.

Synthesis of No_mod-ABDC

No_mod (500 mg) was suspended in a solution of ABDC (0.075 M) in DMF (33 mL) for 72 hours at 120 °C. The solid was subsequently centrifuged and washed with DMF (25 mL, one-hour soaking), water (2 × 25 mL, two-hour soaking) and acetone (25 mL, one-hour soaking; 25 mL, overnight soaking). The solid was dried in air at 80 °C for two hours.

Analytical procedures

Quantitative NMR analysis of hydrolyzed solids was performed with a Bruker AV-500 Avance III spectrometer. About 15 mg of solid was digested for 24 h in 1 mL of 1 M NaOH in D_2O. The NMR tubes were then loaded with the solution, which was filtered through cotton wool to avoid the presence of solid particles in dispersion. Powder X-ray diffraction (PXRD) patterns were collected in the 4-30° 2θ range with a Bruker D8 Avance diffractometer working in reflection geometry and equipped with a LYNXEYE XE detector, using the Cu Kα radiation. The X-ray tube was operated at 40 kV and 40 mA. N_2 sorption isotherms at 77 K were measured with a Quantachrome Nova 2000e analyzer. The samples (about 30-50 mg) were kept overnight in an oven at 100 °C, then activated for four hours under vacuum at 120 °C prior to analysis. BET surface areas were calculated in the 0.001-0.043 P/P_0 range, where all the criteria defined by Gomez-Gualdron et al.[20] were fulfilled. Micropore volume was derived using the t-Plot method in the 0.19-0.52 P/P_0 range. Pore size distribution was determined using the Density Functional theory (DFT) method implemented in the Quantachrome NovaWin software. The kernel implemented in NovaWin software was Non Local DFT (NLDFT)- N_2 - silica equilibrium

transition kernel at 77 K based on a cylindrical pore model. High pressure CO_2 and N_2 excess adsorption isotherms were measured at 283 K (CO_2), 298 K (CO_2 and N_2), 313 K (CO_2) with a Quantachrome iSorb HP1 analyser. The samples (about 150-200 mg) were activated under vacuum with a stepwise procedure keeping them at 60 °C for 1 hour, 80 °C for 1 hour and 120 °C for 4 hours. This procedure was employed in order to prevent abrupt removal of adsorbed solvents (i.e. acetone and water). CO_2 isotherms were fitted using the Dual Site Langmuir equation. N_2 isotherms were fitted using the Langmuir-Freundlich equation (dual site Langmuir-Freundlich was used for No_mod-ABDC). The isosteric heat of CO_2 adsorption (IHA) was calculated by using the linear version of the Clausius-Clapeyron equation in the loading range 0.1-1.0 mmol g^{-1}. Ideal adsorbed solution theory (IAST) CO_2/N_2 selectivity for a 0.15:0.85 CO_2/N_2 mixture in the pressure range 1-5 bar was calculated using the simulated isotherms obtained from the software *IAST++*.[21] Thermogravimetric analysis (TGA) was performed with a TA Instruments SDT-Q600 instrument using alumina cups at and a 5 °C min^{-1} heating rate up to 700 °C in air. Scanning electron microscopy (SEM) was performed with a JEOL 7800F FEG SEM instrument with an acceleration voltage of 7.0 kV. The powders were deposited on carbon sticky tape on an aluminum support and sputtered with chromium (current: 100 mA; time: 30 s; thickness: 2 nm).

Results and Discussion

Fundamental aspects of PSE and PSDE

The basic concepts of PSE and PSDE are shown in Figure 2. Both methods rely on the modification of a pristine MOF matrix (UiO-66 in this work) by exchange of carboxylic species coordinated to the metal clusters with new carboxylic species. There are substantial differences

in the modifications occurring within the porous framework when it is subjected to PSE versus when it is subjected to PSDE.

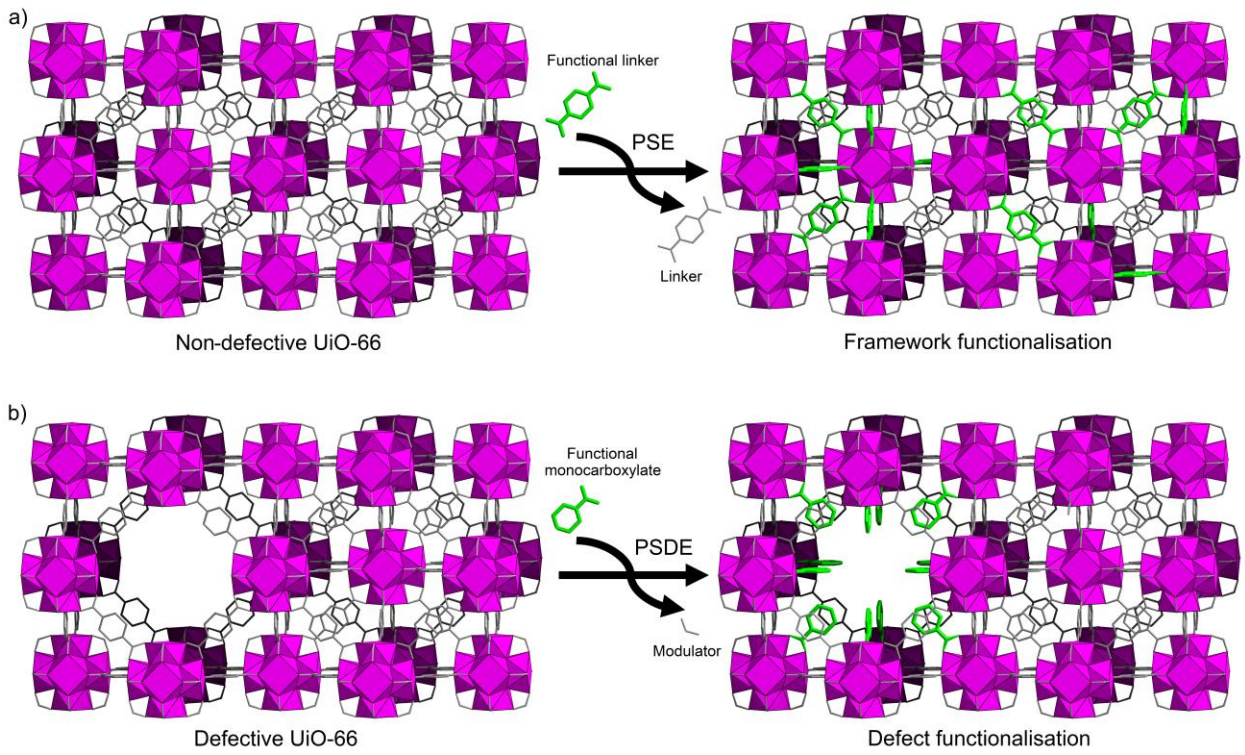

Figure 2. (a) Defect-free UiO-66 undergoes PSE, exchanging one terephthalate linker (represented in grey) with one functional linker (green), which is homogeneously distributed in the structure. (b) UiO-66 containing missing-cluster defects undergoes PSDE, exchanging one modulator unit (grey) with one functional monocarboxylate (green), which is selectively incorporated at defective sites.

PSE (Figure 2a) involves replacement of a dicarboxylic linker (BDC in this work, see Figure 1) by another dicarboxylate having the same size and bearing a functional group (PyDC or ABDC in this work, see Figure 1). The resulting mixed-linker MOF displays homogeneous distribution of functionalized linkers throughout its structure,[22] unless crystallite size is not in the 10-100 μm range, where formation of core-shell structures could be observed.[23] If the new linker

does not bear bulky and heavy functional groups (as is the case of this work), no drastic changes in the porosity of the framework are expected, which allows isolation of the effect of chemical modification on the physical-chemical properties of the framework.

In the case of PSDE (Figure 2b), the exchanged species is a monocarboxylic modulator grafted at a defective site (FA in this work, see Figure 1), which can be replaced by any species containing at least one carboxylic group. Upon complete PSDE of FA, only the defective part of the framework is selectively functionalized and reduction of porosity is expected, due to crowding of the pores. As a result, PSDE has an effect on both the textural features of the MOF and the physical-chemical environment at missing-cluster defective sites. As recently demonstrated, PSE and PSDE compete when defective UiO-66 is soaked in a solution of a terephthalic acid analogue.[19] In order to have pure PSDE, we employed both bare BA and benzoic acid analogues bearing amino functionalities (i.e. PA, NA, AA and ABA, see scheme 1). The amino-functionalized monocarboxylates were selected because of their analogous nature to PyDC and ABDC, which are commonly used linkers for introducing amino functionalities in Zr-MOF frameworks, with the aim of comparing the effect of PSE and PSDE on the CO_2 capture performance. By the use of BA, we aimed at identifying the pore size engineering effect of replacing FA with BA, which has similar size to the other monocarboxylates, but does not possess any nitrogen moieties.

Samples preparation and characterization

A batch of defective UiO-66 (henceforth denoted as FA_mod) was solvothermally prepared using BDC linker in the presence of FA as a modulator. The functionalized materials were then synthesized by solid-liquid PSDE, by soaking FA_mod in a solution of the desired

acid (Scheme 1) in DMF at 80 °C for 24 hours. The structural integrity of the crystalline modified materials was confirmed using PXRD (Figure S1). SEM images do not depict considerable differences, with all the samples displaying the usual octahedral morphology and no evident traces of amorphous matter, corroborating the crystalline nature of the exchanged MOFs (Figures S2-S7). Quantitative NMR analysis of the solids hydrolyzed in alkaline conditions evidenced that FA species grafted at the defective sites of the parental material were almost completely exchanged by benzoic acid analogues (Table 1, Figures S8-S13). In the whole series of materials, the amount of monocarboxylic acid grafted to the defective sites of the parent FA_mod is almost identical. The values of benzoic acid analogue-to-BDC molar ratio fell within a narrow range for all samples from 0.36 to 0.42, allowing us to reliably compare the effect of the grafted species on the sorbents adsorption properties. TGA shows that substitution of FA with amino-functionalized monocarboxylates slightly decreases the thermal stability of the framework, whereas introduction of BA has no visible effect (Figure S14).

Table 1. Chemical composition information of the investigated samples

Sample	**Benzoic acid analogue/BDC**	**Proposed chemical formula**	**Formula weight (g mol^{-1})**
FA_mod	-	$Zr_6O_4(OH)_4(BDC)_{4.96}(FA)_{2.08}$	1586.99
FA_mod-NA	0.39	$Zr_6O_4(OH)_4(BDC)_{4.96}(FA)_{0.17}(NA)_{1.91}$	1734.21
FA_mod-PA	0.40	$Zr_6O_4(OH)_4(BDC)_{4.96}(FA)_{0.16}(PA)_{1.92}$	1734.98
FA_mod-ABA	0.36	$Zr_6O_4(OH)_4(BDC)_{4.96}(FA)_{0.16}(ABA)_{1.92}$	1761.92
FA_mod-AA	0.38	$Zr_6O_4(OH)_4(BDC)_{4.96}(FA)_{0.36}(AA)_{1.72}$	1743.70
FA_mod-BA	0.42	$Zr_6O_4(OH)_4(BDC)_{4.96}(BA)_{2.08}$	1745.26
Sample	**Functional linker/BDC**	**Proposed chemical formula**	**Formula weight (g mol^{-1})**
No_mod	-	$Zr_6O_4(OH)_4(BDC)_6$	1664.02
No_mod-PyDC	0.32	$Zr_6O_4(OH)_4(BDC)_{4.55}(PyDC)_{1.45}$	1665.46
No_mod-ABDC	0.33	$Zr_6O_4(OH)_4(BDC)_{4.51}(ABDC)_{1.49}$	1686.40

Alongside defect-engineered materials, an almost non-defective UiO-66, prepared with no modulator present during synthesis (hereafter No_mod), and functionalized materials resulting from PSE of No_mod with PyDC (No_mod-PyDC) and ABDC (No_mod-ABDC), were synthesized and subsequently characterized. Again, both PXRD (Figure S15) and SEM analysis (Figures S16-S18) do not evidence considerable differences between the starting material and the exchanged MOFs. The degree of linkers exchange lies in a similar range with that observed for defective samples, equaling to 0.32 and 0.33 in No_mod-PyDC and No_mod-ABDC respectively, according to NMR results (Table 1, Figures S19-S21). The incorporation of nitrogen-bearing linkers is further supported by TGA (Figure S22), which shows that decomposition of the framework in No_mod-PyDC and No_mod-ABDC takes place at lower temperatures, in agreement with previous literature reports.[12, 24-25]

Surface area and porosity

Replacement of FA with molecules of higher molecular weight and steric bulk was expected to diminish the porosity and the surface area of the defect-engineered materials. The starting FA_mod has BET surface area of 1520 m^2 g^{-1} and micropore volume of 0.63 cm^3 g^{-1}, owing to the missing clusters defects and the large generated cages present in the material (Figure 3a, Table 2). All the modified defective materials present a BET surface area ranging from 1271 to 1321 m^2 g^{-1}, while their micropore volumes lie between 0.46 and 0.48 cm^3 g^{-1} (Figure 3a, Table 2). Akin porosity properties of the functionalized materials are well anticipated, and they are ascribed to the very close molecular weights and steric bulk of the exchanged acids, and the similar exchange ratios. Nitrogen isotherms in Figure 3a show type 1 sorption behavior,

characteristic of microporous materials[26] and are well fitted to the multi-point BET equation in the relative pressure range of 0.001-0.043 (Figure S23).

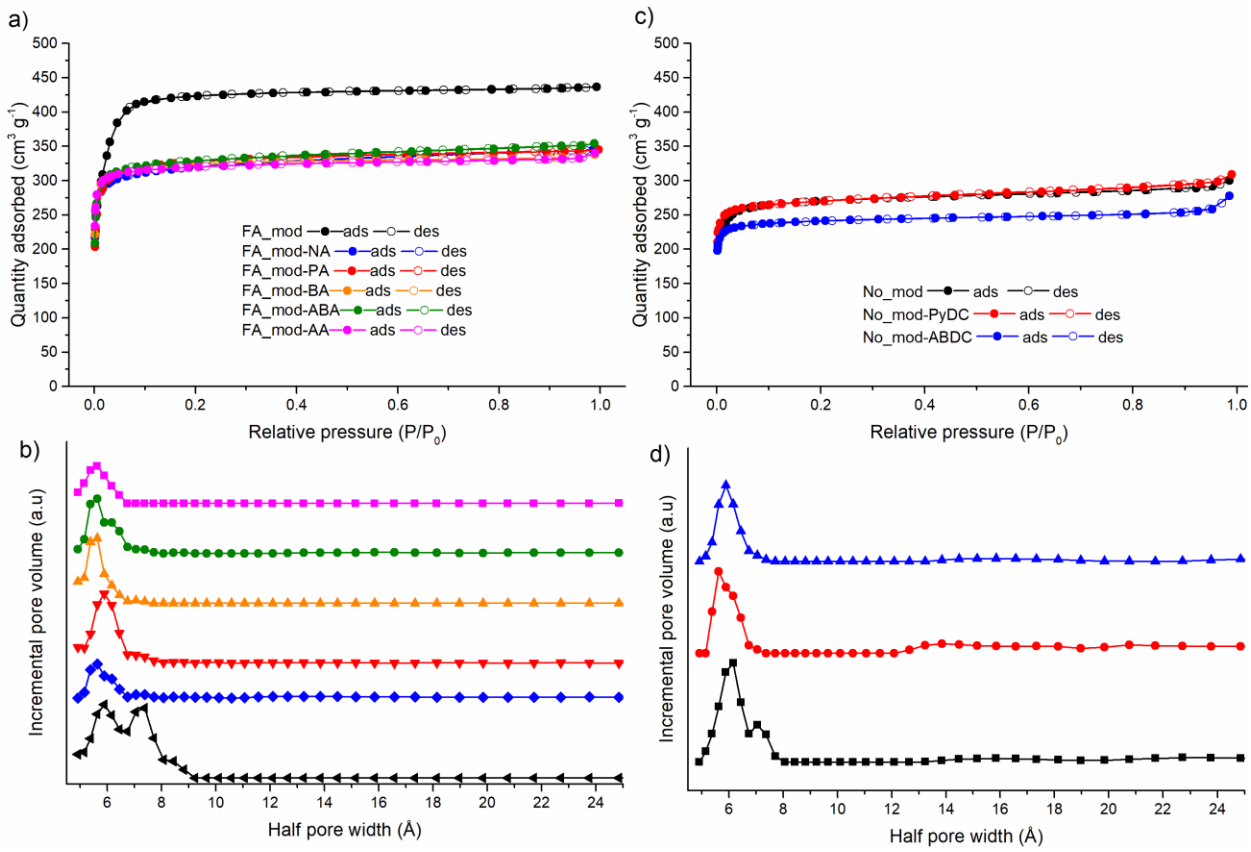

Figure 3. Nitrogen sorption isotherms at 77 K (a) and pore size distribution (b) of FA_mod (black), FA_mod-NA (blue), FA_mod-PA (red), FA_mod-BA (orange), FA_mod-ABA (green) and FA_mod –AA (magenta). Nitrogen sorption isotherm at 77 K (c) and pore size distribution (d) of No_mod (black), No_mod-PyDC (red) and FA_mod-ABDC (blue).

Table 2. Calculated BET Surface area and micropore volume for all the investigated samples.

Sample	BET surface area (m^2 g^{-1})	Micropore volume (cm^3 g^{-1})
FA_mod	1520	0.63
FA_mod-NA	1271	0.46

FA_mod-PA	1310	0.48
FA_mod-ABA	1321	0.48
FA_mod-AA	1303	0.48
FA_mod-BA	1313	0.48

Sample	**BET surface area (m^2 g^{-1})**	**Micropore volume (cm^3 g^{-1})**
No_mod	1084	0.39
No_mod-PyDC	1090	0.39
No_mod-ABDC	981	0.36

During PSDE, NA, PA, BA, ABA and AA replace FA occupying bigger pores at the defective sites of the starting material. As it is evident in Figure 3b, functionalized materials exhibit different shape of pore size distribution (PSD) (determined according to NLDFT), when compared to FA_mod, displays two "porosity peaks" corresponding to pores with radius of about 5.5 and 7.5 Å, respectively, with the latter attributed to the presence of missing-cluster defects. The bimodal shape of FA_mod PSD curve is substituted by monomodal distributions for the modified materials presenting a broader "porosity peak" at a half width of 5.5 Å. We hereby applied NLDFT implementing the same kernel in a series of UiO-66 materials prepared in like manner, permitting us to meaningfully compare the obtained results and the shift in pore sizes. A recent study also shows that NLDFT is able to generate reliable pore size distributions in MOFs.[27] In the case of No_mod, no loss of porosity is observed after the exchange of the parental linkers with PyDC (Figure 3c). A slightly decreased porosity in No_mod-ABDC can be justified by the higher molecular weight and steric demand of ABDC. No considerable differences are observed in the PSD curves shape accordingly (Figure 3d). In the case of No_mod, the presence of a minor peak adjacent to the main peak at 6 Å could be due to the

presence of a small of amount of defects, although the BET surface area of 1084 m^2 g^{-1} is fully consistent with the reported values of non-defective UiO-66.[28]

CO_2 capture performance

Successful functionalization of FA_mod by PSDE allows us to assess the relationships between the nature and orientation of the grafted amino groups and the CO_2 sorption capacity. The single component adsorption isotherms of CO_2 were collected at 283, 298 and 313 K up to 10 bar (Figure 4a, Figures S25-S27). As seen in Figure 4c, FA_mod-ABA and FA_mod-AA achieve a CO_2 uptake of 2.14 mol kg^{-1} at 1 bar and 298 K, significantly enhanced (almost 50% higher) compared to the respective uptake of the parent FA_mod that scarcely approaches 1.44 mol kg^{-1}. Changing the amine group position from *ortho* to *meta* (with respect to the carboxylate) does not induce evident differences between the uptake properties of FA_mod-AA and FA_mod-ABA sorbents. FA_mod-NA and FA_mod-PA also display improved sorption behavior towards CO_2, but not as much as the $–NH_2$ containing materials, with both of them presenting an increase of about 25% at atmospheric conditions. Again, changing the amine group from *ortho* to *meta* position (with respect to the carboxylate) does not appear to affect the CO_2 capacity, as in the case of Cu-based MOFs with nitrogen atoms added into the spacers between two terminal isophthalate moieties.[29]

Interestingly, introduction of BA in exchange for FA enhances the sorption properties as well. FA_mod-BA shows an uptake of 1.93 mol kg^{-1} at 298 K and 1 bar, accounting for an increase of 34% in comparison with FA_mod. Indeed, pore size engineering has been shown to be an efficient strategy to improve CO_2 capture in several studies.[30-31] Grafting of the bulkier BA fills up the large pores present at the defective sites. As a result, CO_2 molecules fit better in the

pores, having higher contact areas and consequently stronger van der Waals forces that lead to improved sorption capacity.[9] In the high pressure regime, FA_mod predictably uptakes more than the modified materials, especially at 283 K (Figure S25), as its superior surface area dominates on the capture mechanism and outperforms the enhanced affinity of its counterparts.

Mixed-linker materials also exhibit higher uptakes than No_mod (Figure 4b). Alike defect-engineered materials, the effect of amine group is more pronounced than pyridinic nitrogen, accounting for an increase of 29% in No_mod-ABDC and 10% in No_mod_PyDC at 298 K and 1 bar (Figure 4c). Defect-free No_mod presents higher CO_2 uptake at lower pressures than FA_mod in agreement with the results obtained by Liang et al.,[32] while the defective material is superior at higher pressures. The highest uptake of both the defect-engineered and mixed-linker materials is achieved by No_mod-ABDC. FA_mod-AA exhibits the highest increase of 48%, if compared to the starting material, of all the analyzed MOFs.

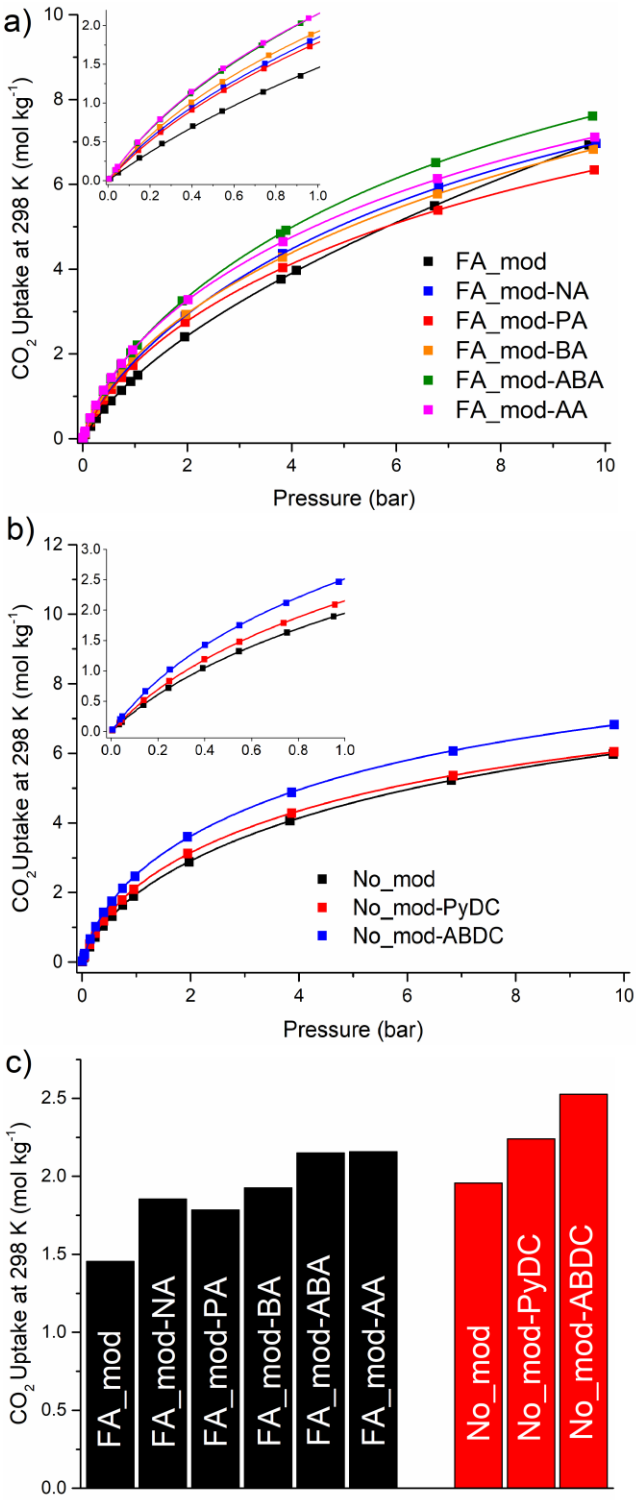

Figure 4. Measured volumetric CO_2 uptakes: (a) CO_2 excess adsorption isotherm at 298 K of FA_mod (black), FA_mod-NA (blue), FA_mod-PA (red), FA_mod-BA (orange), FA_mod-ABA

(green) and FA_mod-AA (magenta), (b) CO_2 excess adsorption isotherm at 298 K of No_mod (black), No_mod-PyDC (red), No_mod-ABDC (blue), (c) CO_2 uptake values at 298 K and 1 bar.

The isosteric heat of CO_2 adsorption (IHA) is a common parameter used to estimate the strength of the interaction between CO_2 and the sorbent surface. IHA was calculated from the CO_2 adsorption isotherms at 283, 298 and 313 K using the Clausius-Claperyon equation. All the defect-engineered materials show higher binding energies than FA_mod, as evidenced by the calculated IHA values (Figure 5a). At near-zero loading, the IHA of functionalized sorbents (24-27 kJ mol^{-1}) is significantly higher the starting FA_mod (17.6 kJ mol^{-1}). The improved dispersion interactions is probably the main factor behind the rise in IHA.[33] FA_mod-BA also shows significantly increased IHA, leading us to the conclusion that stronger interaction forces could also be due to structural parameters and not exclusively owed to the nitrogen incorporation. FA_mod-ABA and FA_mod-AA, that capture the highest amount of CO_2, have analogous IHA values to FA_mod-BA, FA_mod-NA and FA_mod-PA and their superior uptake behavior cannot be directly rationalized by IHA. In agreement with this, moderate IHA values were observed in the channels of a high-performing MOF material lined by basic amine groups and the high CO_2 uptake was not accompanied by strong adsorbent-adsorbate interactions.[34] It appears that, at the degree of functionalization we achieve, IHA does not change significantly. One notable feature evident from Figure 4a is that IHA of defect-engineered materials decreases when loading increases from 0.1 to 1 mol kg^{-1}, while IHA of FA_mod remains practically constant over the same loading range. This behavior is likely due to the modification of the pore system upon PSDE. Future computational studies could allow us to gain deeper insight into the interaction between CO_2 and defect-engineered materials. We should also note that error bars of amine functionalized materials and FA_mod-BA overlap, indicating that the difference between the

means of IHA is not statistically significant. CO_2/N_2 selectivity, as determined by the ideal adsorbed solution theory (IAST) for a 0.15:0.85 mixture at 298 K, also appears to increase in the nitrogen functionalized materials, both in pyridine form and amine form (Figure 5b). Following the same pattern of the CO_2 uptake measurements, FA_mod-ABA and FA_MOD-AA have the highest selectivity, achieving a value close to 22, much higher than the value of 14 of FA_mod. Interaction of CO_2 molecules with the amine group via hydrogen bonding or between the N lone pair and the C atom of CO_2, probably cause the enhanced affinity of these materials for CO_2.[33] Notably, the selectivity is barely improved in FA_mod-BA. Given its substantially higher CO_2 uptake, it is inferred that pure pore size engineering could also be favorable for N_2, eventually resulting in a moderate selectivity improvement. This is further supported by the superior N_2 uptake of FA_mod-BA at low pressures (Figure S29). In the family of non-defective materials, no considerable differences are observed in both IHA and IAST selectivity of No_mod and its mixed-linker derivatives (Figure 5c-d). Overall, the non-defective materials display slightly higher selectivity than the defective materials. This could partly be explained by the lower porosity of non-defective frameworks: it is known that ultramicropores (5 - 7 Å) are more selective towards CO_2, compared to supermicropores (7 - 20 Å).[9] Another factor that is likely to play a role is the absence of part of the hexanuclear Zr clusters in the defective materials: both experiments and simulations have demonstrated that the -OH groups on the clusters are important adsorption sites for CO_2.[35]

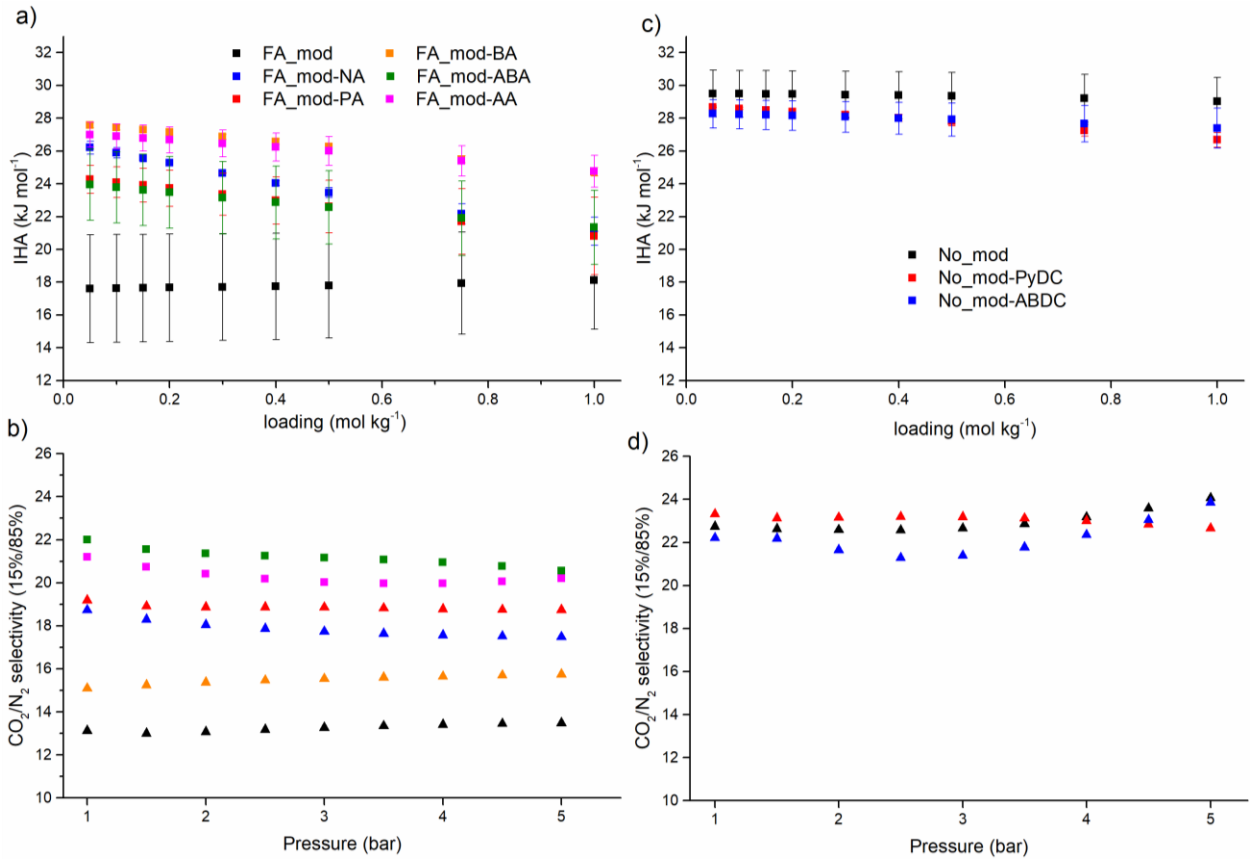

Figure 5. Isosteric heat of CO_2 adsorption as a function of loading (a) and IAST selectivity CO_2 /N_2 (15:85) (b) of FA_mod (black), FA_mod-NA (blue), FA_mod-PA (red), FA_mod-BA (orange), FA_mod-ABA (green) and FA_mod –AA (magenta). Isosteric heat of CO_2 adsorption as a function of loading (c) and IAST selectivity CO_2 /N_2 (15:85) (d) of No_mod (black), No_mod-PyDC (red), FA_mod-ABDC (blue).

Conclusion

The systematic investigation performed in the present study demonstrates that post-synthetic exchange of modulator species grafted at defective sites with various nitrogen-containing monocarboxylates enhances the overall CO_2 capture performance of defective UiO-66. NH_2-functionalised sorbents showed superior performance than the materials bearing heterocyclic

nitrogen, although the position of the nitrogen groups did not appear to significantly effect on the gas uptake properties. A CO_2 uptake increase of 48%, compared to the pristine FA_mod, was achieved by defect-functionalized FA_mod-AA at ambient conditions, exceeding the respective value achieved by framework functionalized No_mod-ABDC (29%, compared to No_mod). Notably, the PSDE approach leads to improvement of CO_2/N_2 selectivity, whereas framework functionalization by PSE does not. Simple tailoring of the pore size through exchange of FA with BA also improved the overall CO_2 uptake, but the selectivity improved only fractionally, implying that amino groups are necessary to enhance affinity for CO_2. The successful employment of defect-engineering approach towards enhanced properties unveils the method's potential.

Considering the dynamic and versatile nature of defects in Zr-MOFs and the variety of guest molecules that could be hosted in larger pores via PSDE, we reveal that our defect-engineering approach entails numerous opportunities for further development as an important tool for tuning the physical-chemical properties of MOFs. Ongoing investigation in our group is aimed at further exploiting PSDE to improve the CO_2 capture performance of defective Zr-MOFs, both introducing functional groups that are not accessible via linker modification in UiO-66, e.g. aliphatic amines, and functionalizing frameworks based on less chemically versatile linkers than BDC.

ASSOCIATED CONTENT

Supporting Information.

The following files are available free of charge:

- Supporting information file (PDF).

AUTHOR INFORMATION

Corresponding Authors

* marco.taddei@swansea.ac.uk; e.andreoli@swansea.ac.uk

Funding Sources

The authors gratefully acknowledge the financial support provided by the Sêr Cymru Chair Programme (A.R.B.). The European Union's Horizon 2020 research and innovation programme under the Marie Skłodowska-Curie grant agreement No 663830 (M.T.), and the Engineering and Physical Sciences Research Council (EPSRC) for funding through the First Grant scheme EP/R01910X/1 (M.T.). The Welsh Government is also acknowledged for the Sêr Cymru II Recapturing Talent Fellowship (E.K.) partly funded by the European Regional Development Fund (ERDF). This work is also part of the Reduce Industrial Carbon Emissions (RICE) and Flexible Integrated Energy Systems (FLEXIS) operations funded by Welsh European Funding Office (WEFO), also partly funded by the ERDF. We would like to acknowledge the assistance provided by the Swansea University AIM Facility, which was funded in part by the EPSRC EP/M028267/1, the ERDF through the Welsh Government grant 80708, and the Sêr Solar project via the Welsh Government. Financial support was also provided the Robert A. Welch Foundation (C-0002).

REFERENCES

1. *Reducing UK emissions – 2018 Progress Report to Parliament*; 2018.

2. Bui, M.; Adjiman, C. S.; Bardow, A.; Anthony, E. J.; Boston, A.; Brown, S.; Fennell, P. S.; Fuss, S.; Galindo, A.; Hackett, L. A.; Hallett, J. P.; Herzog, H. J.; Jackson, G.; Kemper, J.; Krevor, S.; Maitland, G. C.; Matuszewski, M.; Metcalfe, I. S.; Petit, C.; Puxty, G.; Reimer, J.; Reiner, D. M.; Rubin, E. S.; Scott, S. A.; Shah, N.; Smit, B.; Trusler, J. P. M.; Webley, P.; Wilcox, J.; Mac Dowell, N., Carbon capture and storage (CCS): the way forward. *Energy Environ. Sci.* **2018**, *11* (5), 1062-1176.

3. Porter, R. T. J.; Fairweather, M.; Kolster, C.; Mac Dowell, N.; Shah, N.; Woolley, R. M., Cost and performance of some carbon capture technology options for producing different quality CO_2 product streams. *Int. J. Greenh. Gas Con.* **2017**, *57*, 185-195.

4. Rao, A. B.; Rubin, E. S., A Technical, Economic, and Environmental Assessment of Amine-Based CO_2 Capture Technology for Power Plant Greenhouse Gas Control. *Environ. Sci. Technol.* **2002**, *36* (20), 4467-4475.

5. Patel, H. A.; Byun, J.; Yavuz, C. T., Carbon Dioxide Capture Adsorbents: Chemistry and Methods. *ChemSusChem* **2017**, *10* (7), 1303-1317.

6. Sumida, K.; Rogow, D. L.; Mason, J. A.; McDonald, T. M.; Bloch, E. D.; Herm, Z. R.; Bae, T.-H.; Long, J. R., Carbon Dioxide Capture in Metal–Organic Frameworks. *Chem. Rev.* **2012**, *112* (2), 724-781.

7. Yichao, L.; Chunglong, K.; Qiuju, Z.; Liang, C., Metal-Organic Frameworks for Carbon Dioxide Capture and Methane Storage. *Adv. Energy Mater.* **2017,** *7* (4), 1601296.

8. Bai, Y.; Dou, Y.; Xie, L.-H.; Rutledge, W.; Li, J.-R.; Zhou, H.-C., Zr-based metal-organic frameworks: design, synthesis, structure, and applications. *Chem. Soc. Rev.* **2016,** *45* (8), 2327-2367.

9. Oschatz, M.; Antonietti, M., A search for selectivity to enable CO_2 capture with porous adsorbents. *Energy Environ. Sci.* **2018,** *11* (1), 57-70.

10. Ethiraj, J.; Albanese, E.; Civalleri, B.; Vitillo, J. G.; Bonino, F.; Chavan, S.; Shearer, G. C.; Lillerud, K. P.; Bordiga, S., Carbon Dioxide Adsorption in Amine-Functionalized Mixed-Ligand Metal–Organic Frameworks of UiO-66 Topology. *ChemSusChem* **2014,** *7* (12), 3382-3388.

11. Abid, H. R.; Shang, J.; Ang, H.-M.; Wang, S., Amino-functionalized Zr-MOF nanoparticles for adsorption of CO_2 and CH_4. *Int. J. Smart Nano Mater* **2013,** *4* (1), 72-82.

12. Barkhordarian, A. A.; Kepert, C. J., Two new porous UiO-66-type zirconium frameworks; open aromatic N-donor sites and their post-synthetic methylation and metallation. *J. Mater. Chem. A* **2017**, *5* (11), 5612-5618.

13. Li, L.-J.; Liao, P.-Q.; He, C.-T.; Wei, Y.-S.; Zhou, H.-L.; Lin, J.-M.; Li, X.-Y.; Zhang, J.-P., Grafting alkylamine in UiO-66 by charge-assisted coordination bonds for carbon dioxide capture from high-humidity flue gas. *J. Mater. Chem. A* **2015**, *3* (43), 21849-21855.

14. Taddei, M., When defects turn into virtues: The curious case of zirconium-based metal-organic frameworks. *Coord. Chem. Rev.* **2017**, *343*, 1-24.

15. Park, H.; Kim, S.; Jung, B.; Park, M. H.; Kim, Y.; Kim, M., Defect Engineering into Metal–Organic Frameworks for the Rapid and Sequential Installation of Functionalities. *Inorg. Chem.* **2018**, *57* (3), 1040-1047.

16. Taylor, J. M.; Dekura, S.; Ikeda, R.; Kitagawa, H., Defect Control To Enhance Proton Conductivity in a Metal–Organic Framework. *Chem. Mater.* **2015**, *27* (7), 2286-2289.

17. Feng, X.; Jena, H. S.; Leus, K.; Wang, G.; Ouwehand, J.; Van Der Voort, P., l-proline modulated zirconium metal organic frameworks: Simple chiral catalysts for the aldol addition reaction. *J. Catal.* **2018**, *365*, 36-42.

18. Shearer, G. C.; Vitillo, J. G.; Bordiga, S.; Svelle, S.; Olsbye, U.; Lillerud, K. P., Functionalizing the Defects: Postsynthetic Ligand Exchange in the Metal Organic Framework UiO-66. *Chem. Mater.* **2016**, *28* (20), 7190-7193.

19. Taddei, M.; Wakeham, R. J.; Koutsianos, A.; Andreoli, E.; Barron, A. R., Post-Synthetic Ligand Exchange in Zirconium-Based Metal–Organic Frameworks: Beware of The Defects! *Angew. Chem. Int. Ed.* **2018**, *57* (36), 11706-11710.

20. Gómez-Gualdrón, D. A.; Moghadam, P. Z.; Hupp, J. T.; Farha, O. K.; Snurr, R. Q., Application of Consistency Criteria To Calculate BET Areas of Micro- And Mesoporous Metal–Organic Frameworks. *J. Am. Chem. Soc.* **2016**, *138* (1), 215-224.

21. Lee, S.; Lee, J. H.; Kim, J., User-friendly graphical user interface software for ideal adsorbed solution theory calculations. *Korean J. Chem. Eng.* **2018**, *35* (1), 214-221.

22. Fluch, U.; Paneta, V.; Primetzhofer, D.; Ott, S., Uniform distribution of post-synthetic linker exchange in metal–organic frameworks revealed by Rutherford backscattering spectrometry. *Chem. Commun.* **2017**, *53* (48), 6516-6519.

23. Boissonnault, J. A.; Wong-Foy, A. G.; Matzger, A. J., Core–Shell Structures Arise Naturally During Ligand Exchange in Metal–Organic Frameworks. *J. Am. Chem. Soc.* **2017**, *139* (42), 14841-14844.

24. Chavan, S. M.; Shearer, G. C.; Svelle, S.; Olsbye, U.; Bonino, F.; Ethiraj, J.; Lillerud, K. P.; Bordiga, S., Synthesis and Characterization of Amine-Functionalized Mixed-Ligand Metal–Organic Frameworks of UiO-66 Topology. *Inorg. Chem.* **2014,** *53* (18), 9509-9515.

25. Taddei, M.; Tiana, D.; Casati, N.; van Bokhoven, J. A.; Smit, B.; Ranocchiari, M., Mixed-linker UiO-66: structure–property relationships revealed by a combination of high-resolution powder X-ray diffraction and density functional theory calculations. *Phys. Chem. Chem. Phys.* **2017,** *19* (2), 1551-1559.

26. Lowell, S., Shields, J.E., Thomas, M.A., Thommes, M., *Characterization of Porous Solids and Powders: Surface Area, Pore Size and Density*. Springer Netherlands: 2004; Vol. 16.

27. Sonnauer, A.; Hoffmann, F.; Fröba, M.; Kienle, L.; Duppel, V.; Thommes, M.; Serre, C.; Férey, G.; Stock, N., Giant Pores in a Chromium 2,6-Naphthalenedicarboxylate Open-Framework Structure with MIL-101 Topology. *Angew. Chem. Int. Ed.* **2009,** *48* (21), 3791-3794.

28. Shearer, G. C.; Chavan, S.; Bordiga, S.; Svelle, S.; Olsbye, U.; Lillerud, K. P., Defect Engineering: Tuning the Porosity and Composition of the Metal–Organic Framework UiO-66 via Modulated Synthesis. *Chem. Mater.* **2016,** *28* (11), 3749-3761.

29. Song, C.; Hu, J.; Ling, Y.; Feng, Y.; Krishna, R.; Chen, D.-l.; He, Y., The accessibility of nitrogen sites makes a difference in selective CO_2 adsorption of a family of isostructural metal–organic frameworks. *J. Mater. Chem. A* **2015,** *3* (38), 19417-19426.

30. Wang, J.; Heerwig, A.; Lohe, M. R.; Oschatz, M.; Borchardt, L.; Kaskel, S., Fungi-based porous carbons for CO_2 adsorption and separation. *J. Mater. Chem.* **2012,** *22* (28), 13911-13913.

31. Yiyin, M.; Danke, C.; Pan, H.; Yi, G.; Yulong, Y.; Wen, Y.; Xinsheng, P., Hierarchical Mesoporous Metal–Organic Frameworks for Enhanced CO_2 Capture. *Chem. Eur. J.* **2015,** *21* (43), 15127-15132.

32. Liang, W.; Coghlan, C. J.; Ragon, F.; Rubio-Martinez, M.; D'Alessandro, D. M.; Babarao, R., Defect engineering of UiO-66 for CO_2 and H_2O uptake – a combined experimental and simulation study. *Dalton Trans.* **2016,** *45* (11), 4496-4500.

33. Vaidhyanathan, R.; Iremonger, S. S.; Shimizu, G. K. H.; Boyd, P. G.; Alavi, S.; Woo, T. K., Direct Observation and Quantification of CO_2 Binding Within an Amine-Functionalized Nanoporous Solid. *Science* **2010,** *330* (6004), 650-653.

34. Nandi, S.; Maity, R.; Chakraborty, D.; Ballav, H.; Vaidhyanathan, R., Preferential Adsorption of CO_2 in an Ultramicroporous MOF with Cavities Lined by Basic Groups and Open-Metal Sites. *Inorg. Chem.* **2018,** *57* (9), 5267-5272.

35. Wu, H.; Chua, Y. S.; Krungleviciute, V.; Tyagi, M.; Chen, P.; Yildirim, T.; Zhou, W., Unusual and Highly Tunable Missing-Linker Defects in Zirconium Metal–Organic Framework UiO-66 and Their Important Effects on Gas Adsorption. *J. Am. Chem. Soc.* **2013,** *135* (28), 10525-10532.

TABLE OF CONTENTS GRAPHIC

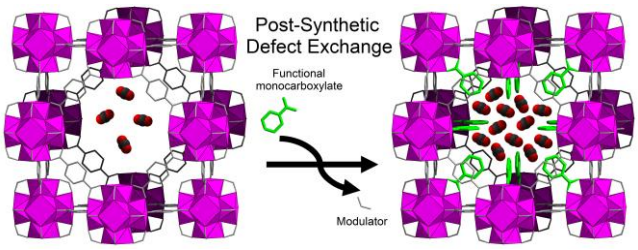

A new approach to enhancing the CO_2 capture performance of defective UiO-66 via post-synthetic defect exchange

Athanasios Koutsianos,[1] Ewa Kazimierska,[1] Andrew R. Barron,[1,2,3] Marco Taddei,[1] and Enrico Andreoli[1]**

[1] Energy Safety Research Institute, Swansea University, Fabian Way, Swansea, SA1 8EN, UK

[2] Department of Chemistry, Rice University, Houston, Texas, 77005, USA

[3] Department of Materials Science and Nanoengineering, Rice University, Houston, Texas, 77005, USA

Supporting Information

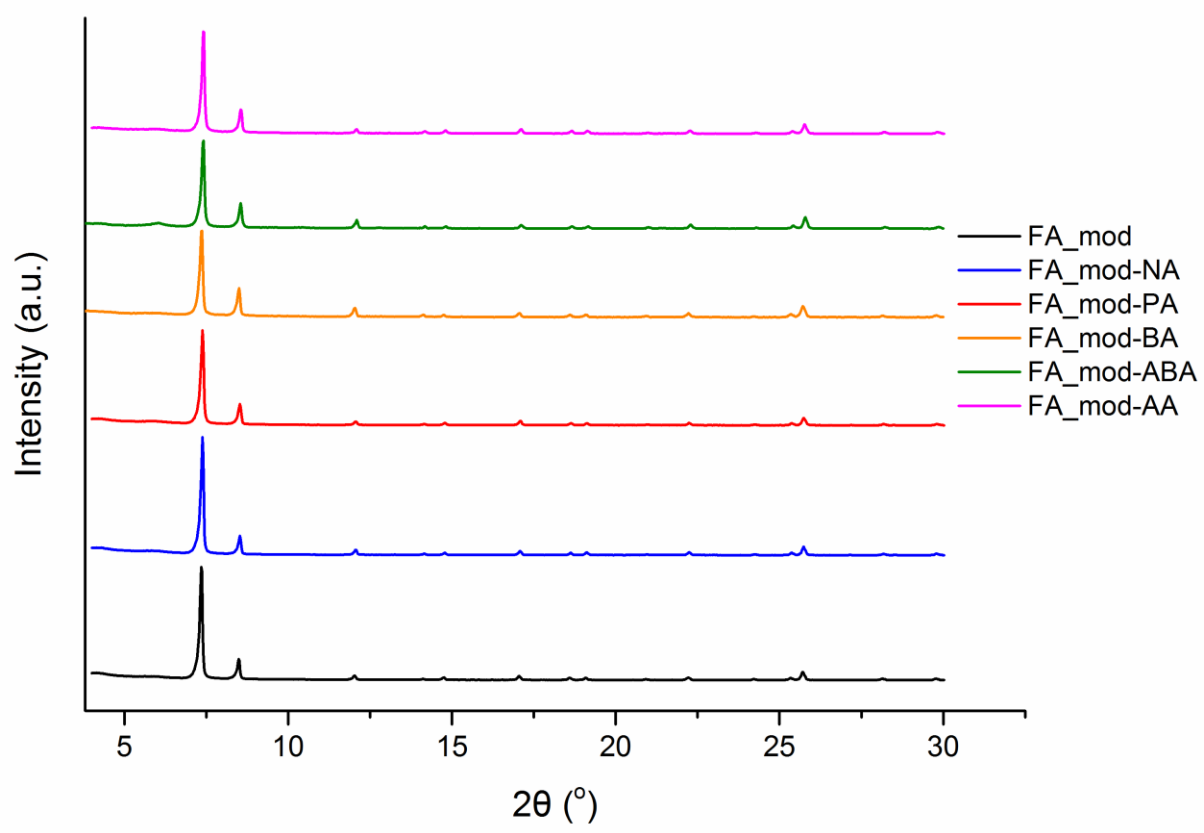

Figure S1. PXRD patterns of defective materials series

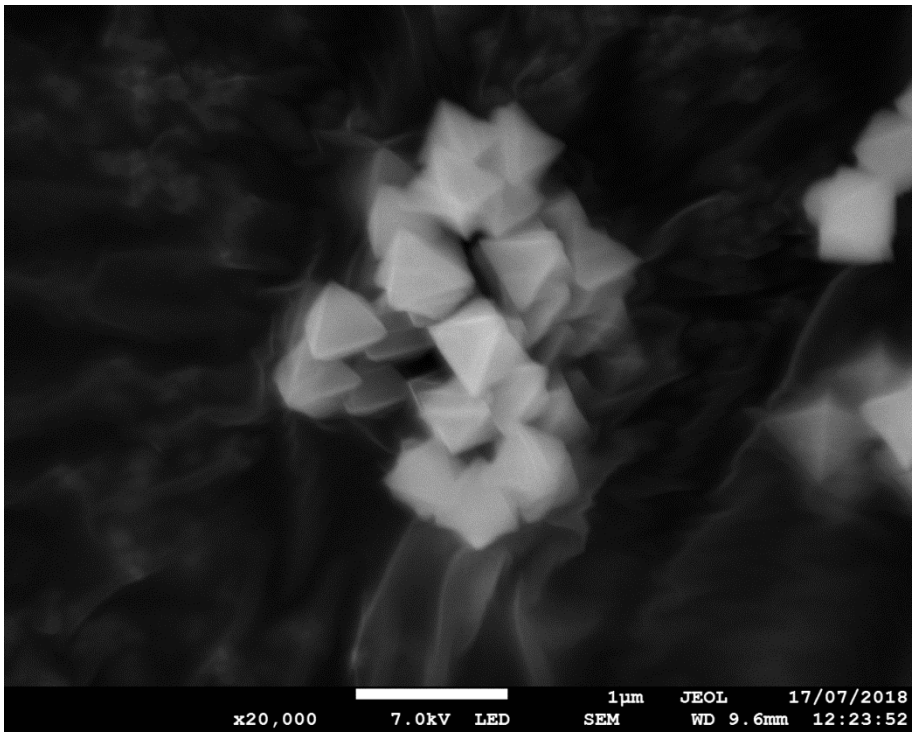

Figure S2. SEM micrograph of FA_mod. Scale bar is 1 µm

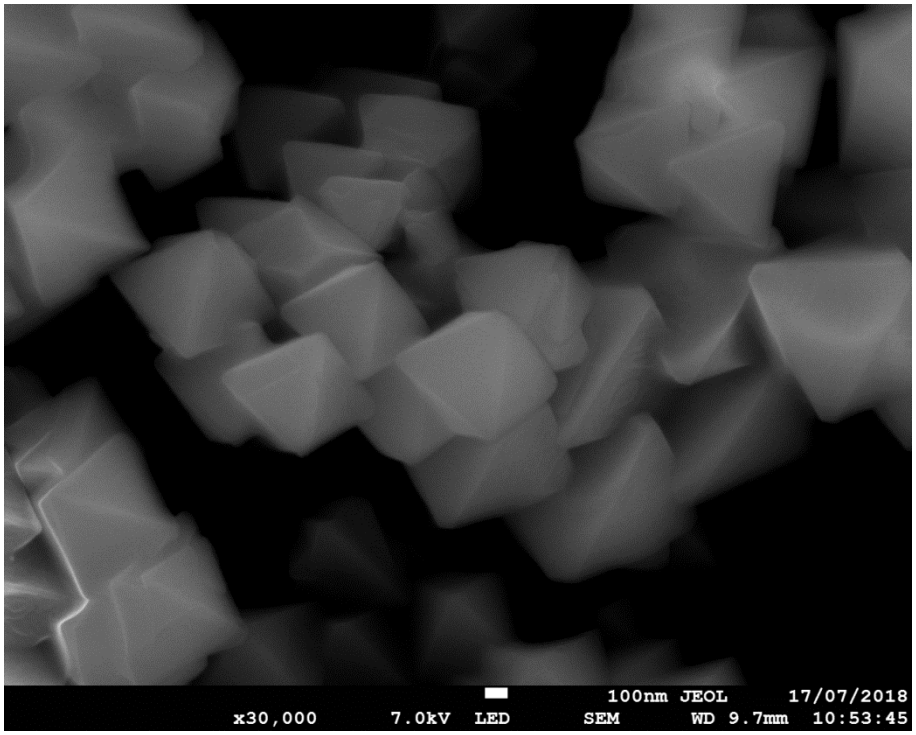

Figure S3. SEM micrograph of FA_mod-NA. Scale bar is 100 nm

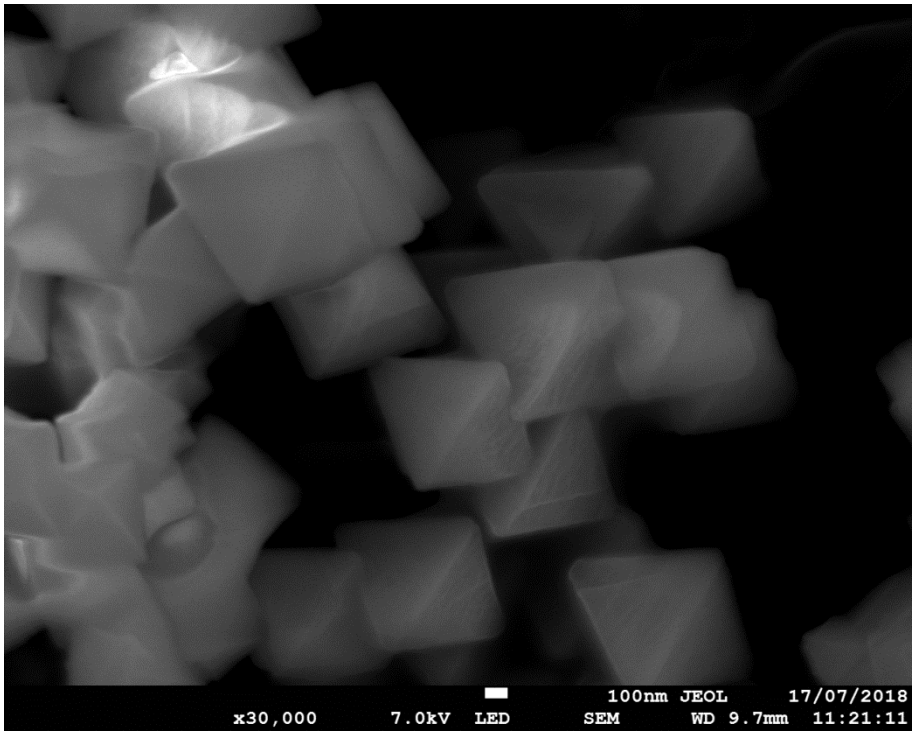

Figure S4. SEM micrograph of FA_mod-PA. Scale bar is 100 nm

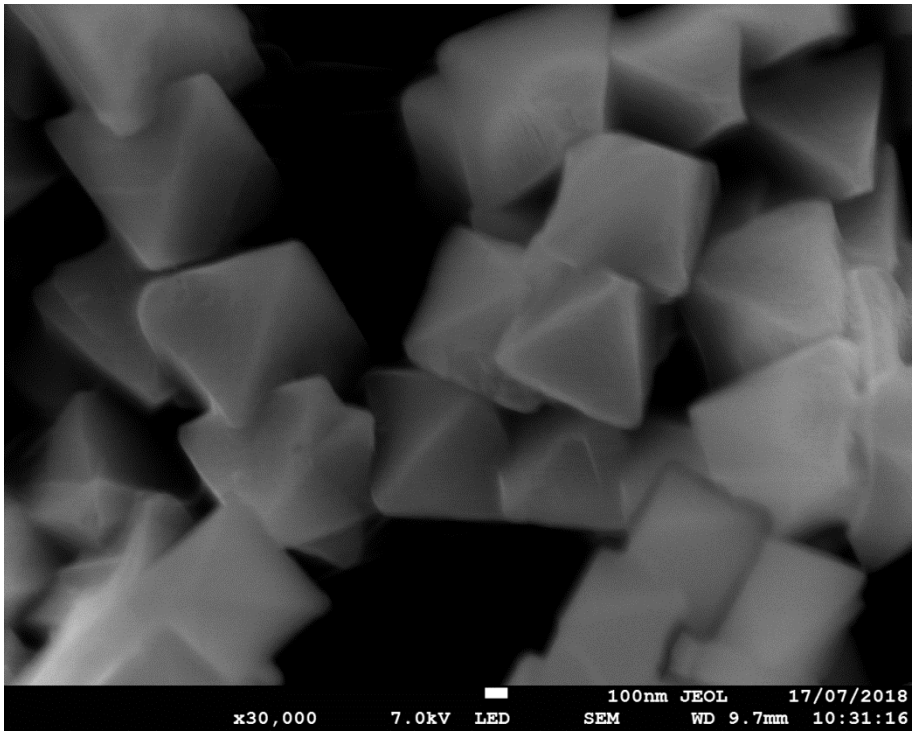

Figure S5. SEM micrograph of FA_mod-BA. Scale bar is 100 nm

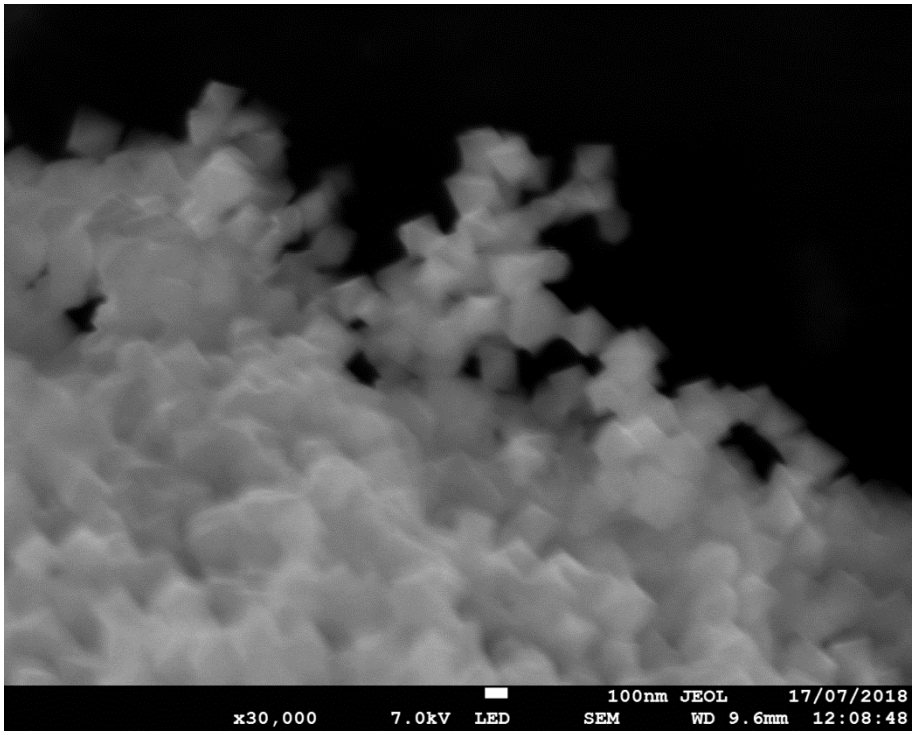

Figure S6. SEM micrograph of FA_mod-ABA. Scale bar is 100 nm

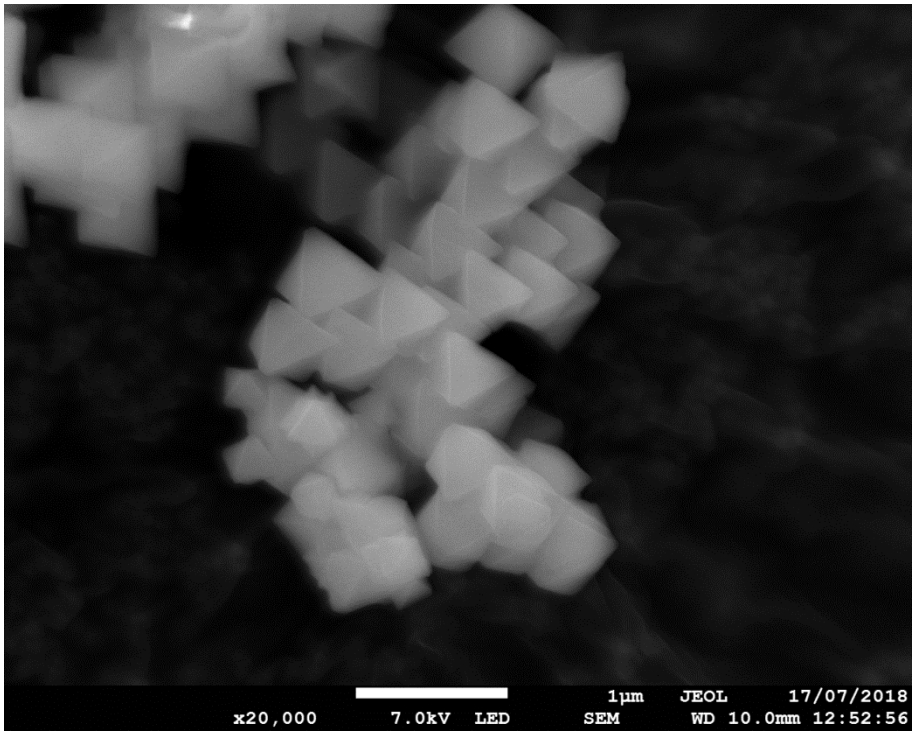

Figure S7. SEM micrograph of FA_mod-AA. Scale bar is 1 µm

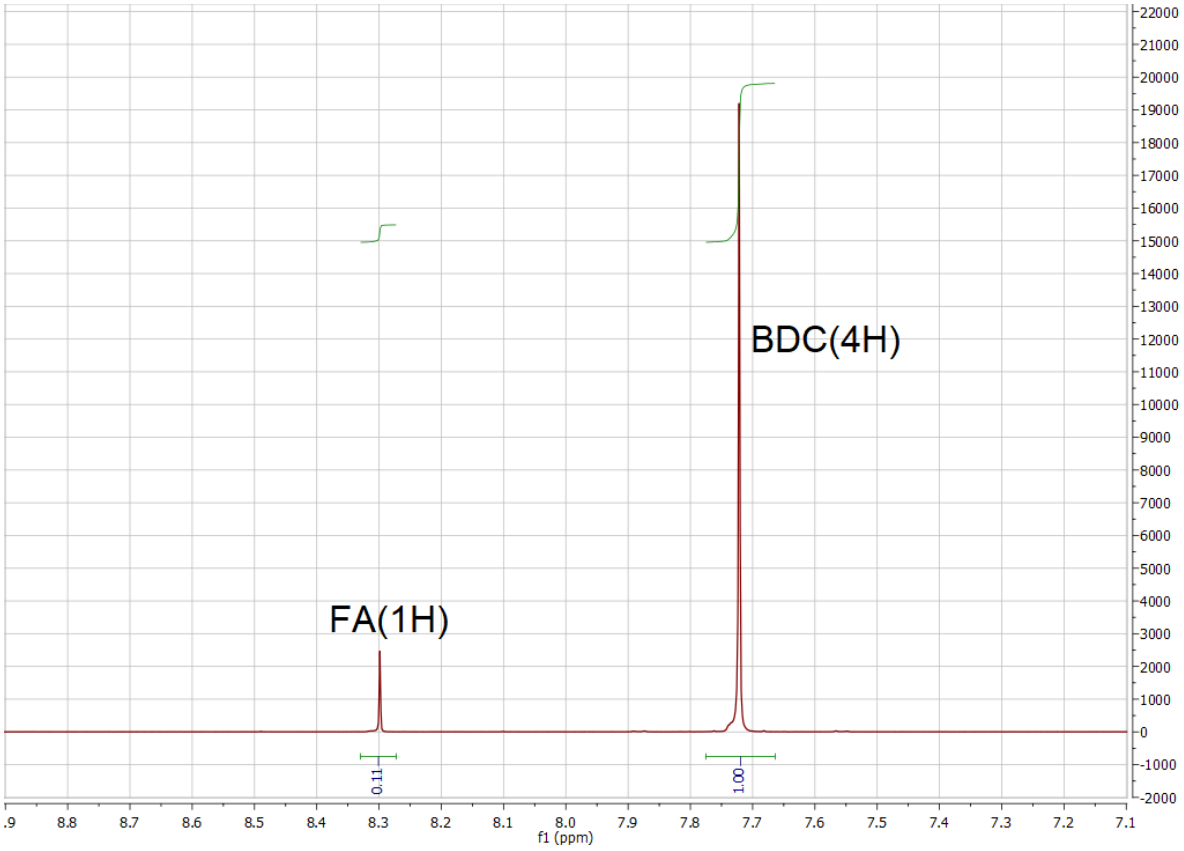

Figure S8. ^{1}H NMR spectrum of FA_mod

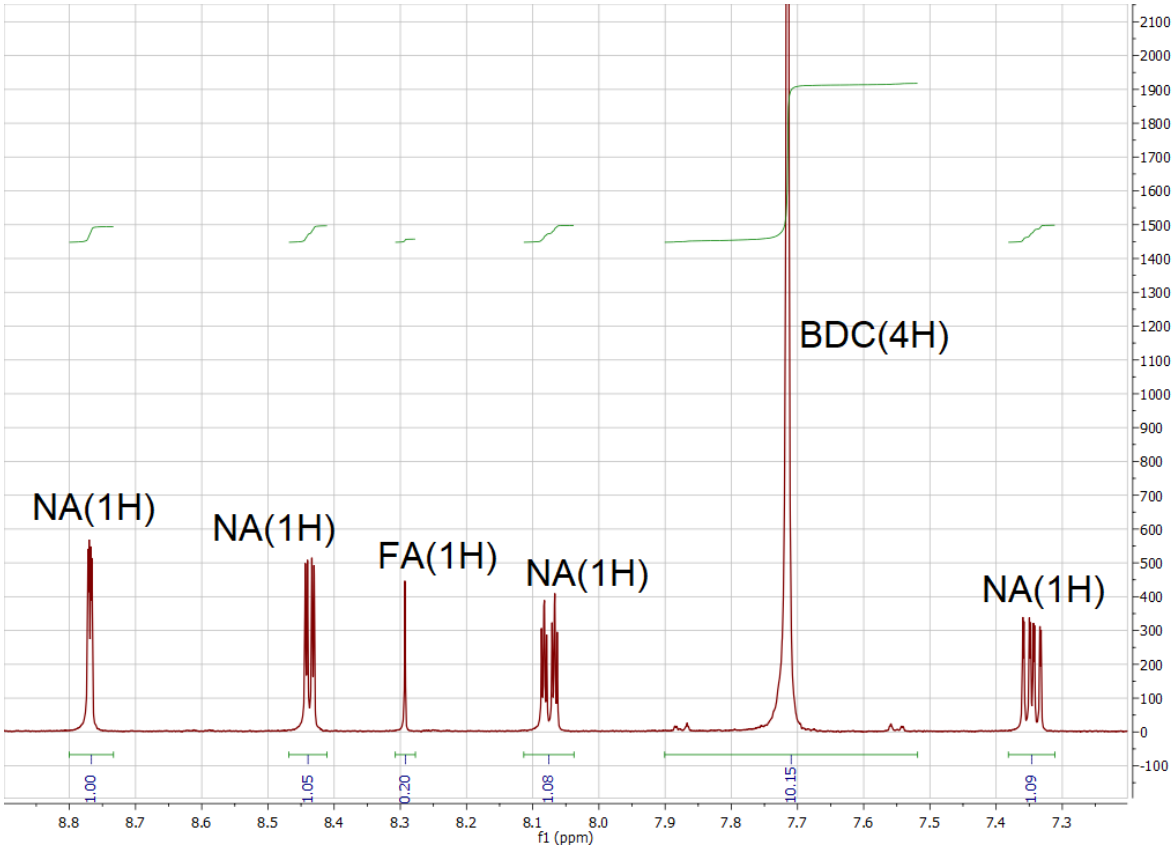

Figure S9. ^{1}H NMR spectrum of FA_mod-NA

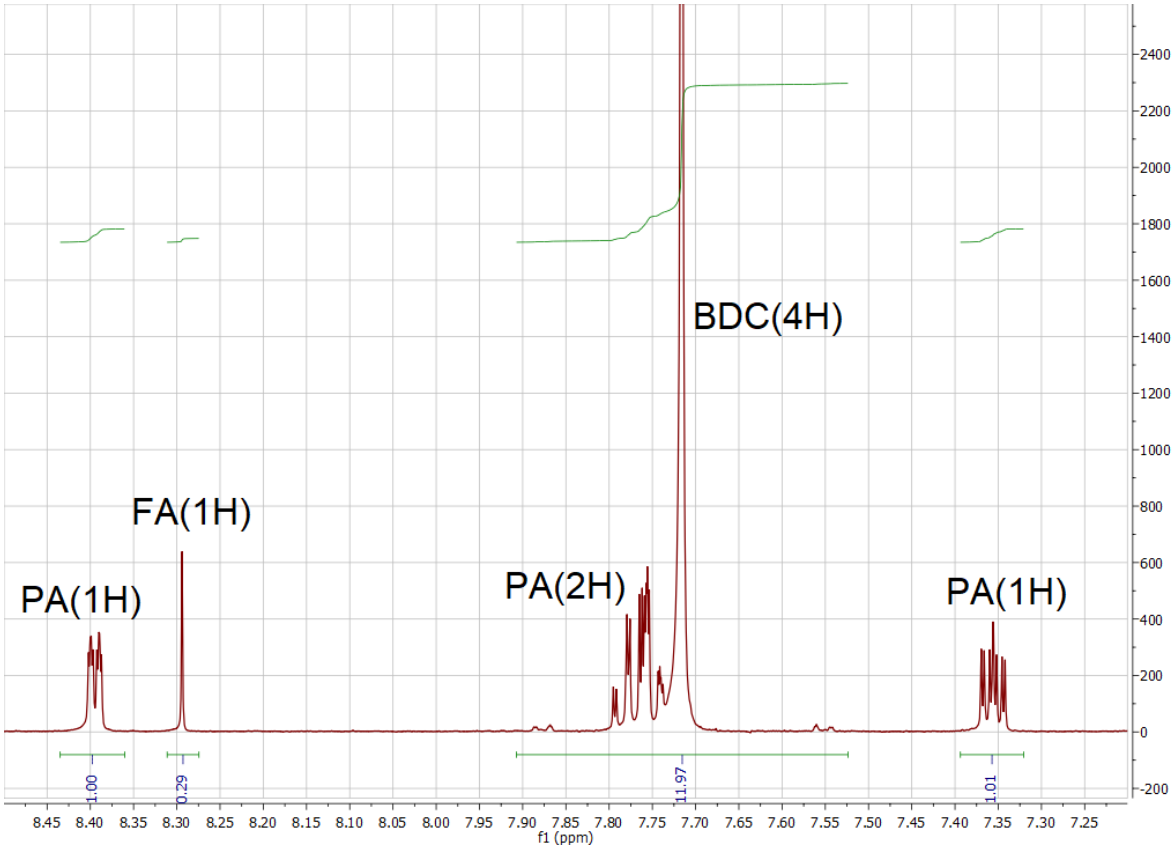

Figure S10. ^{1}H NMR spectrum of FA_mod-PA

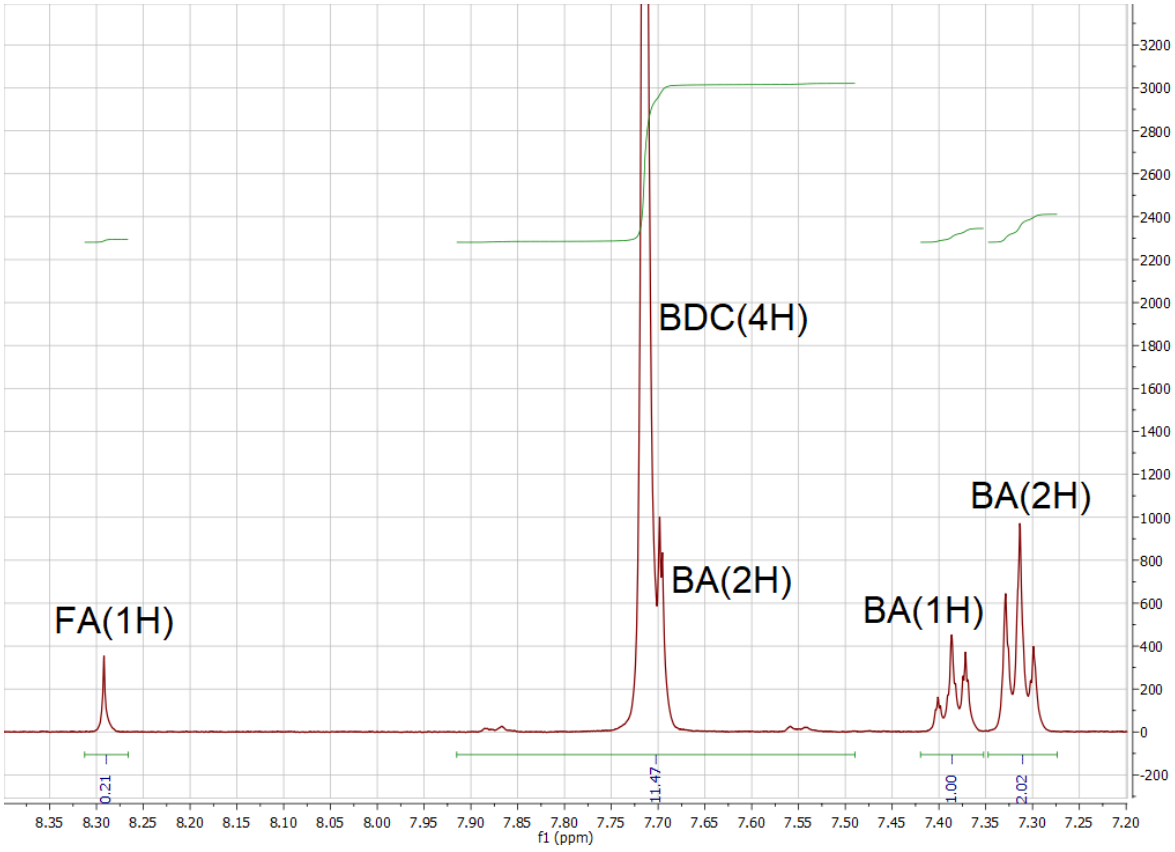

Figure S11. ^{1}H NMR spectrum of FA_mod-BA

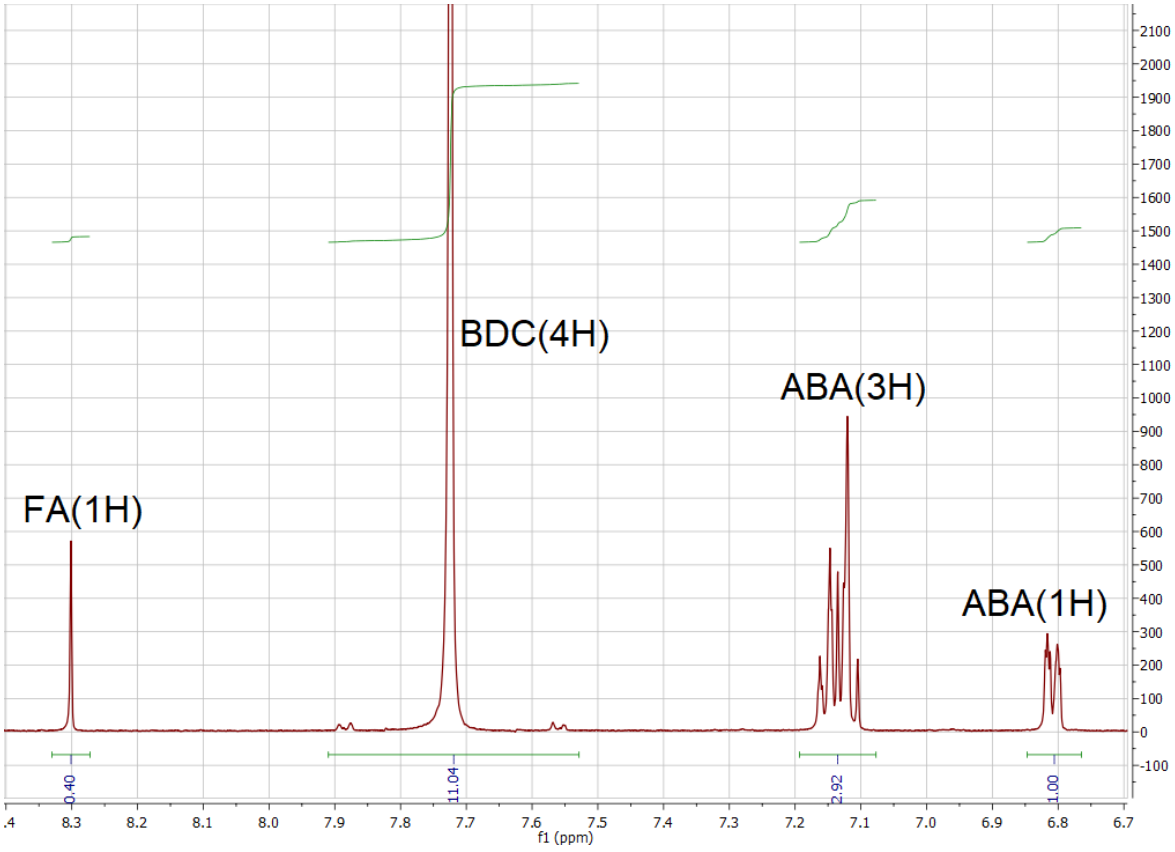

Figure S12. ^{1}H NMR spectrum of FA_mod-ABA

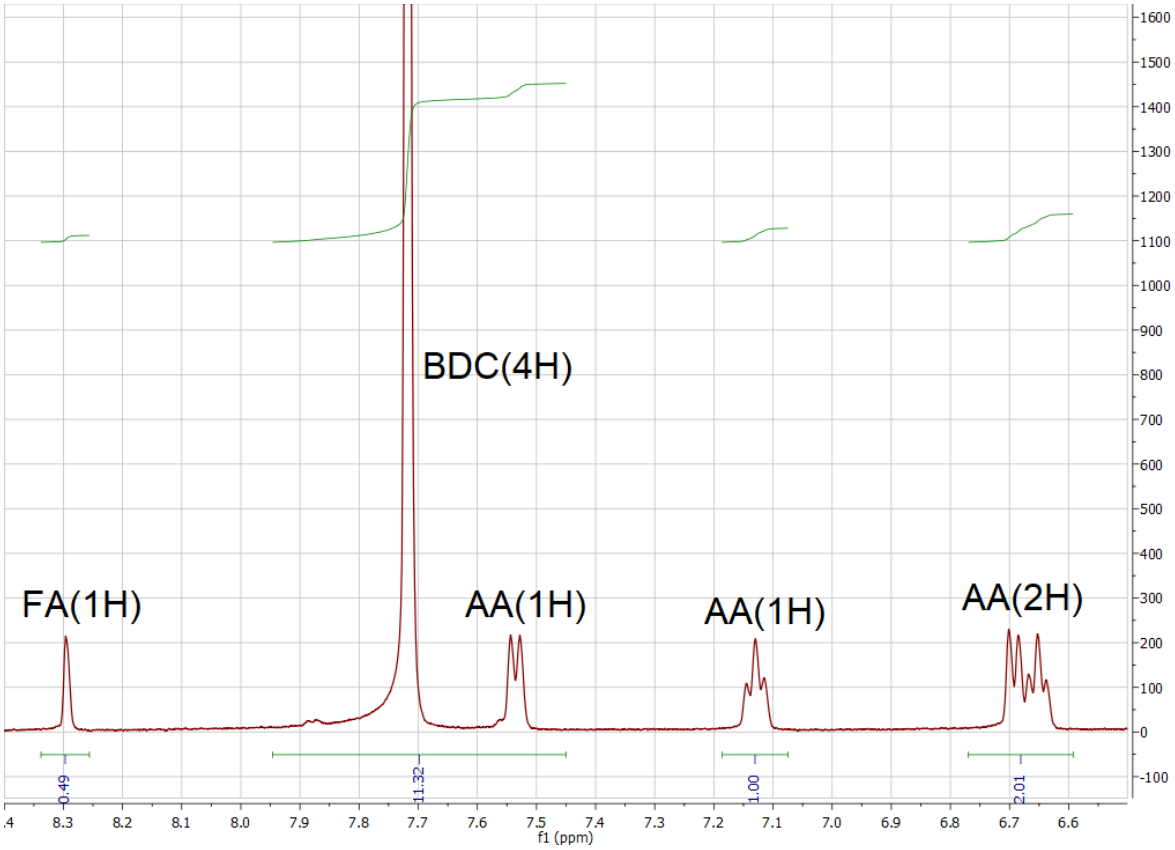

Figure S13. ^{1}H NMR spectrum of FA_mod-AA

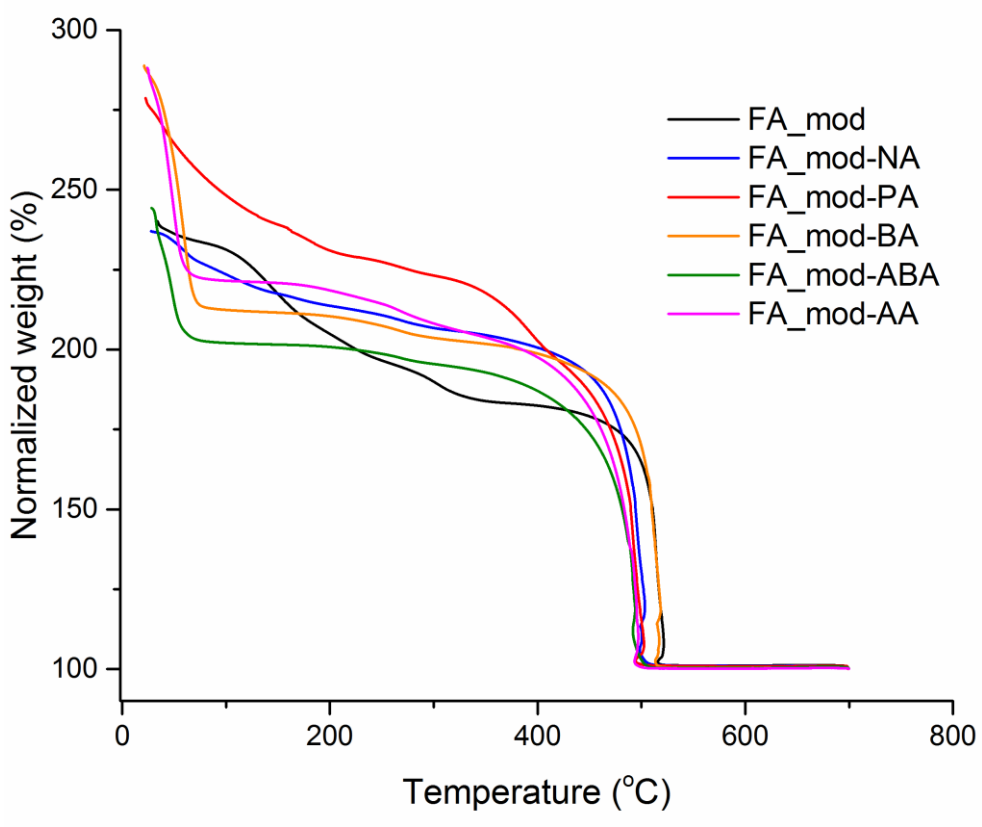

Figure S14. Comparison of the TGA curves of the defective materials

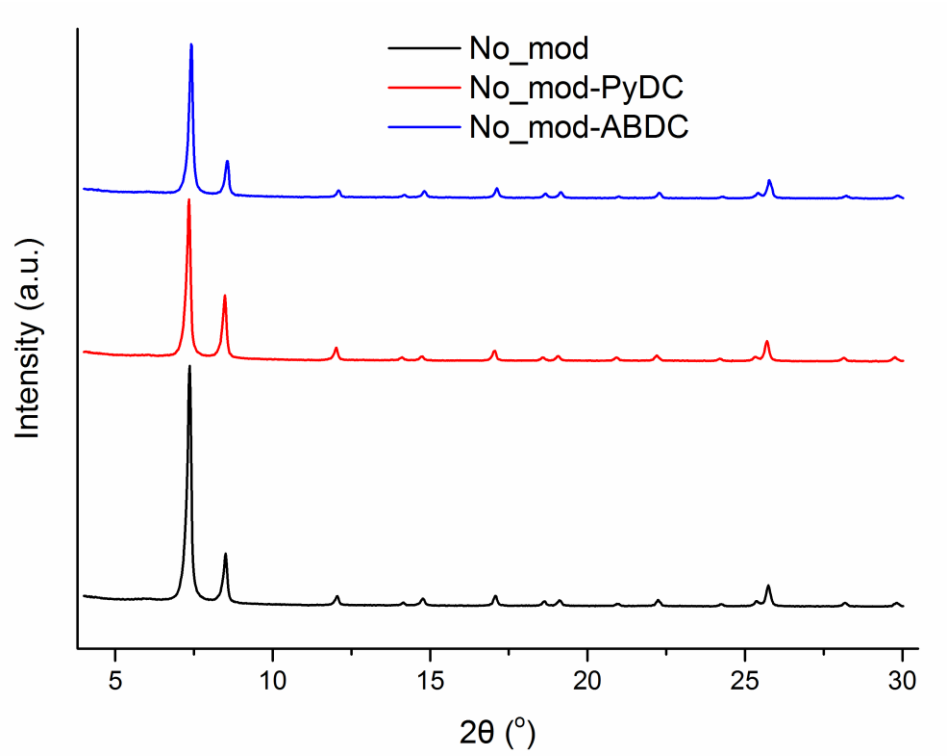

Figure S15. PXRD patterns of non-defective materials series

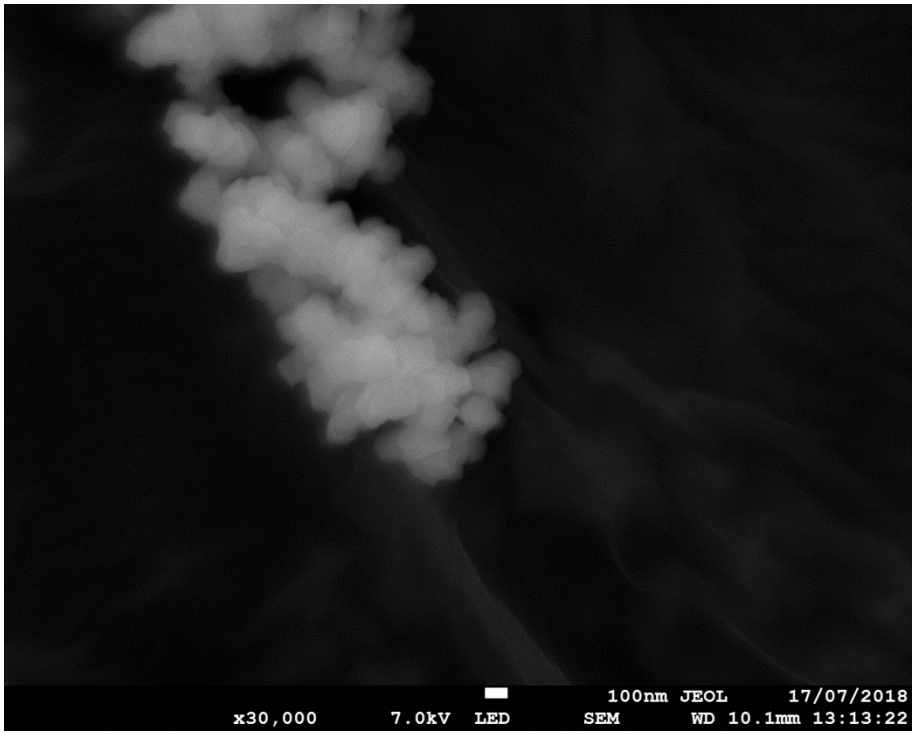

Figure S16. SEM micrograph of No_mod. Scale bar is 100 nm

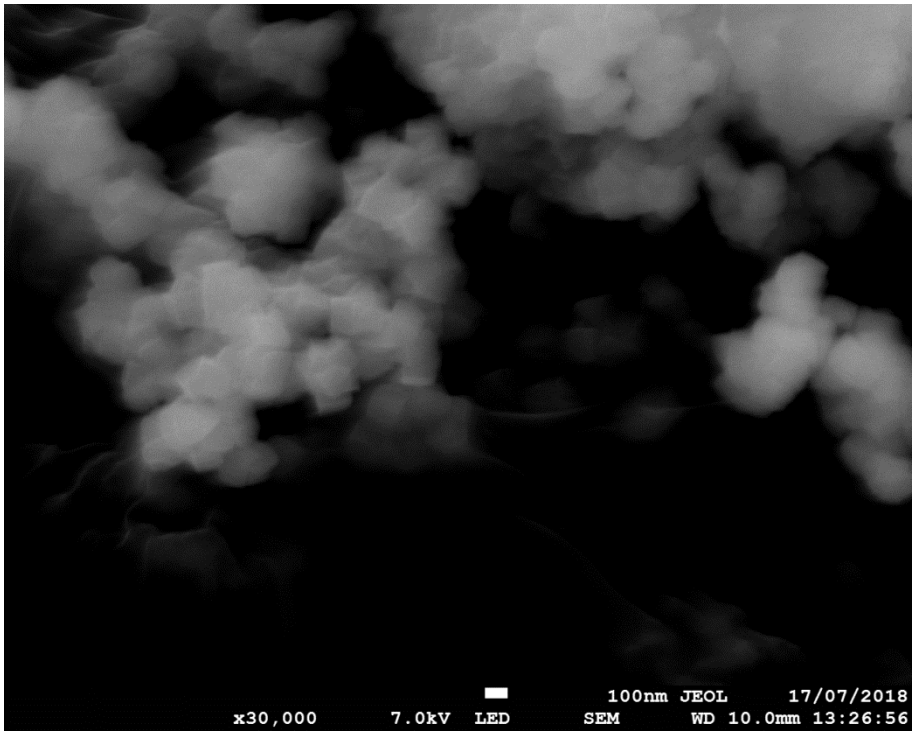

Figure S17. SEM micrograph of No_mod-PyDC. Scale bar is 100 nm

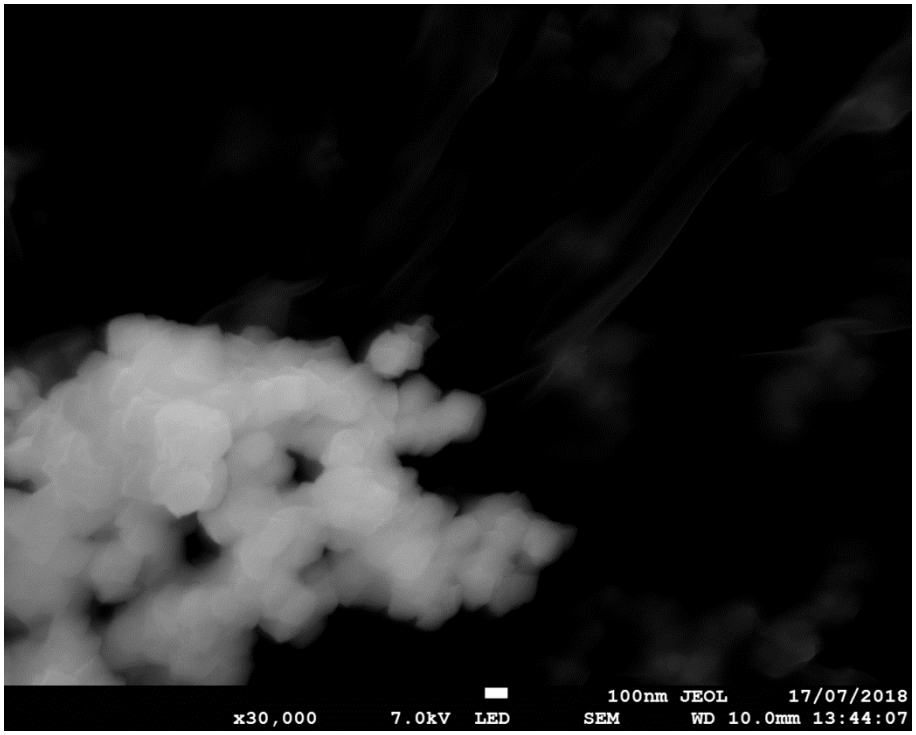

Figure S18. SEM micrograph of No_mod-ABDC. Scale bar is 100 nm

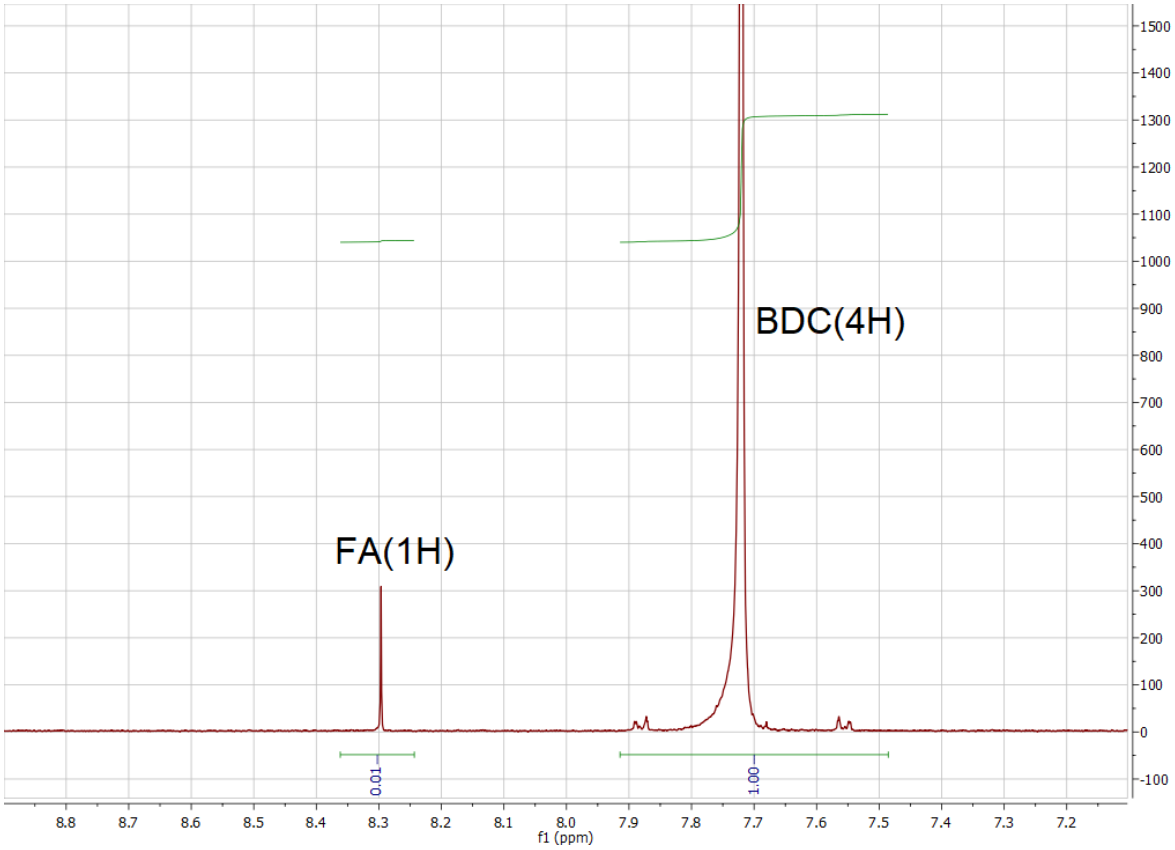

Figure S19. ^{1}H NMR spectrum of No_mod

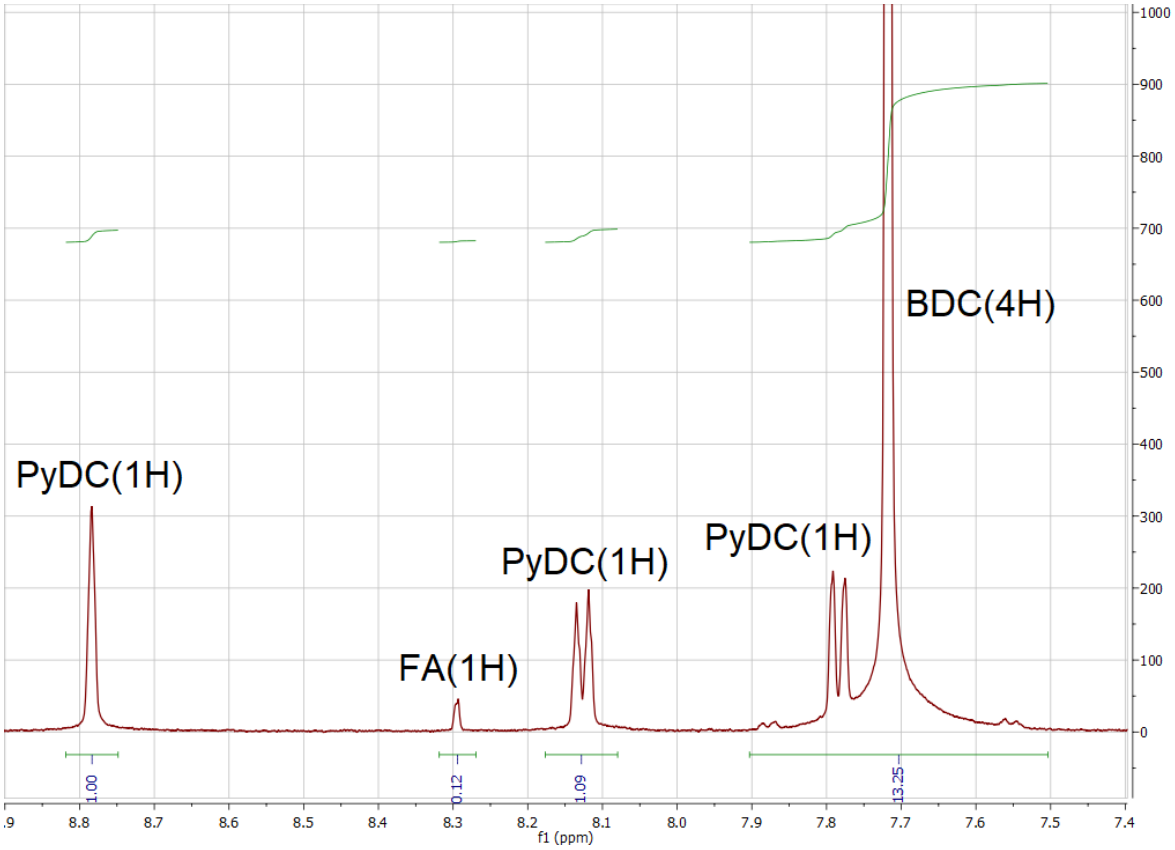

Figure S20. ^{1}H NMR spectrum of No_mod-PyDC

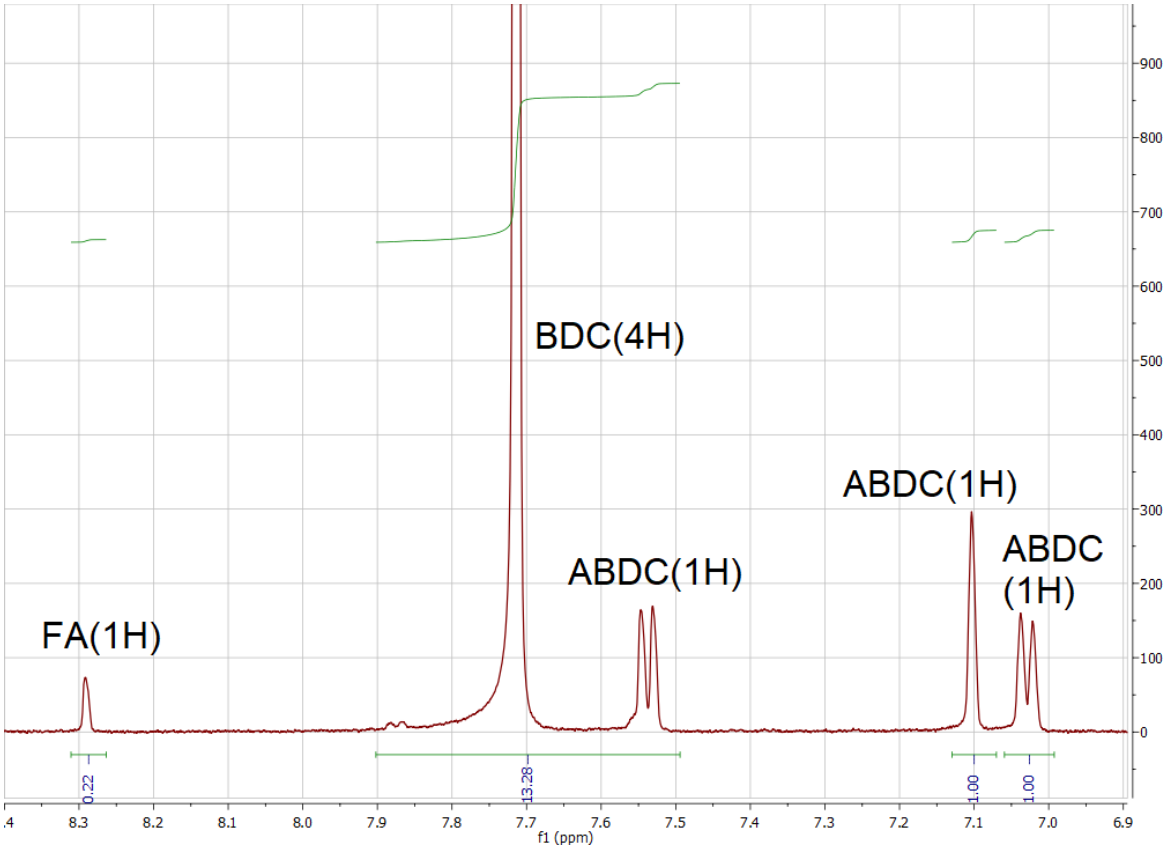

Figure S21. ^{1}H NMR spectrum of No_mod-ABDC

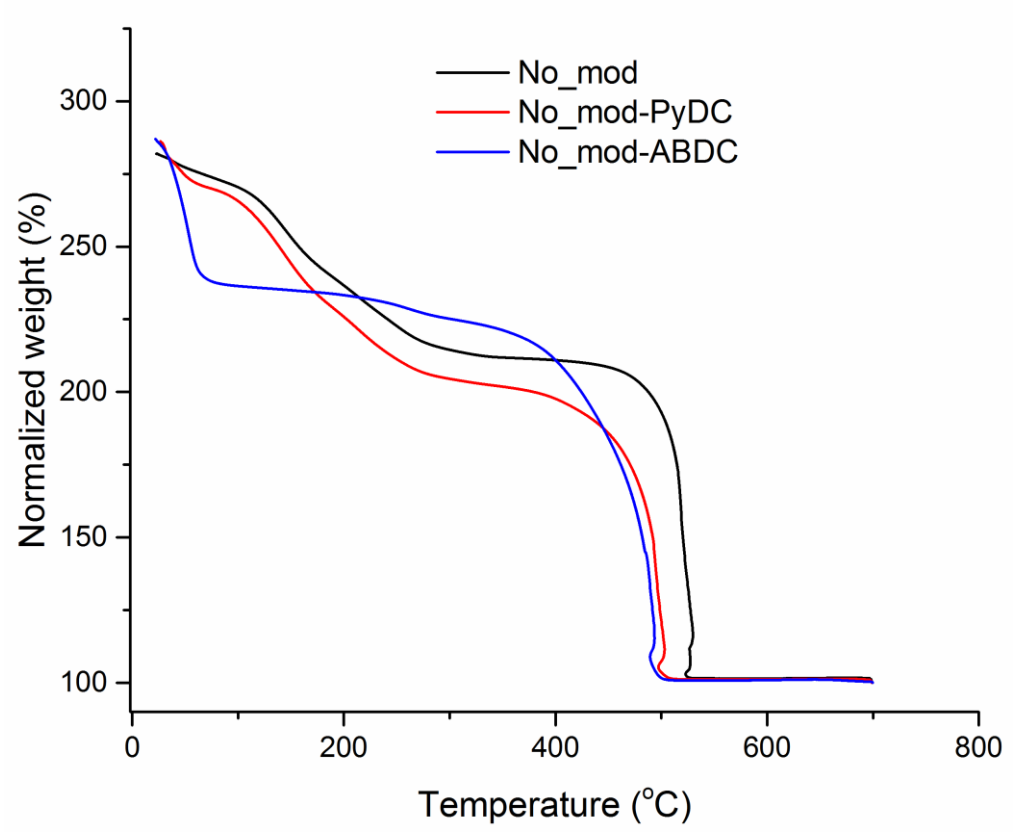

Figure S22. Comparison of the TGA curves of the non- defective series

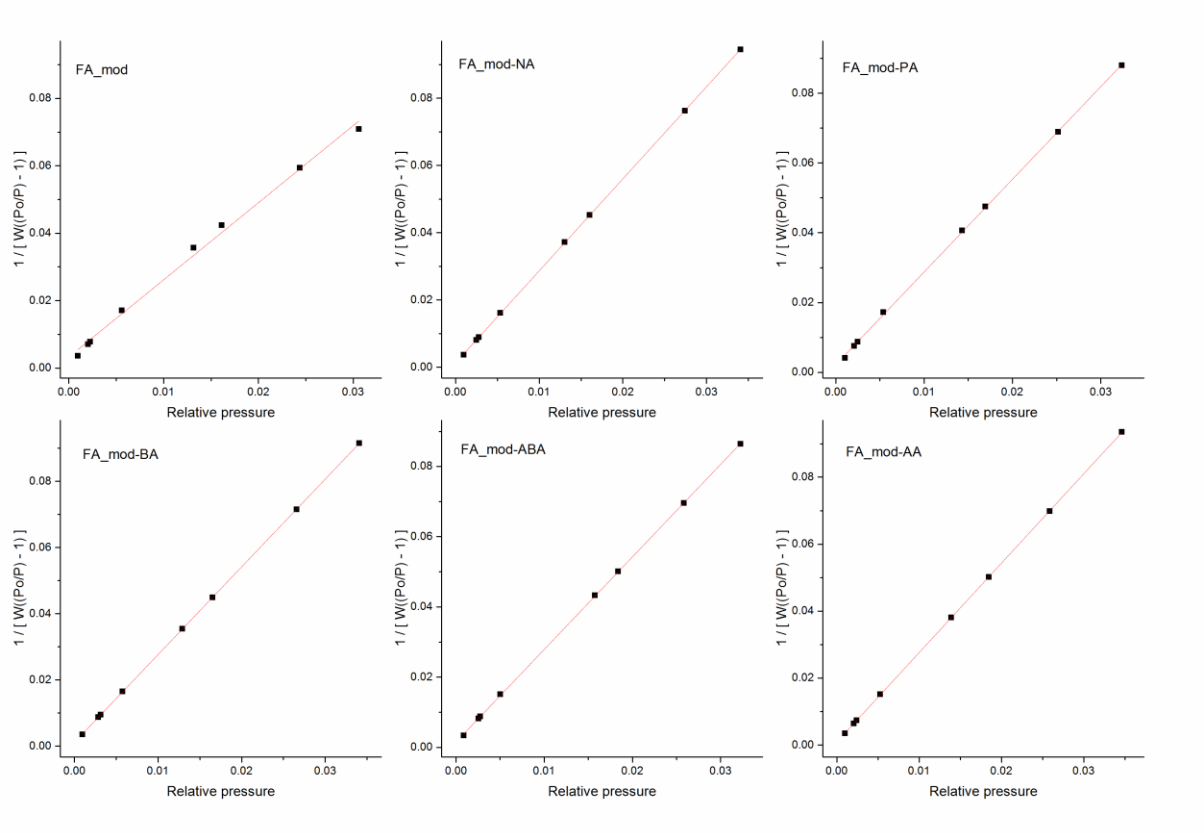

Figure S23. Linearization of the N_2 adsorption isotherms of the defective materials according to the BET model

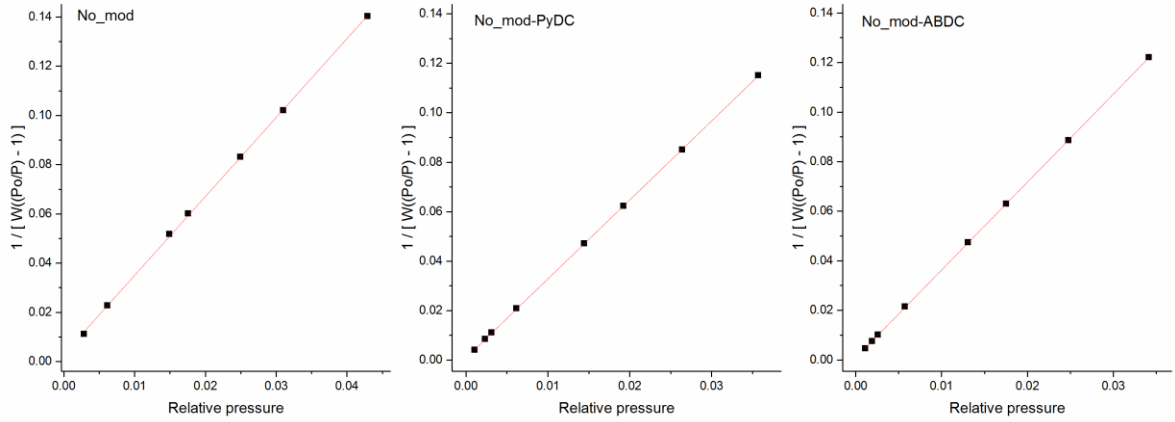

Figure S24. Linearization of the N_2 adsorption isotherms of No_mod, No_mod-PyDC and No_mod-ABDC according to the BET model

Isosteric Heats of Adsorption calculation

In order to calculate the isosteric heats of adsorption (IHA) the dual-site Langmuir model (Equation 1) was used to fit the CO_2 adsorption isotherms at 283, 298 and 313 K with the Origin software. IHA values were then determined using the integrated form of the Clausius-

Clapeyron equation (Equation 2) by calculating the slope of ln(p) vs 1/T for each loading.[1] The standard deviation for the error of the linear regression equation was also calculated using Microsoft Excel.

$$n = \frac{q_{sat,A}\, k_A\, p}{1 + k_A\, p} + \frac{q_{sat,B}\, k_B\, p}{1 + k_B\, p} \qquad (1)$$

$$\ln p_n = \left(\frac{IHA}{R}\right)\left(\frac{1}{T}\right) + C \qquad (2)$$

where n is the loading in mol/kg, q_{sat} is the saturation loading for site A or B, k_A and k_B are the Langmuir parameters associated with site A and B respectively (bar^{-1}), p is the pressure (bar) and T the temperature (K).

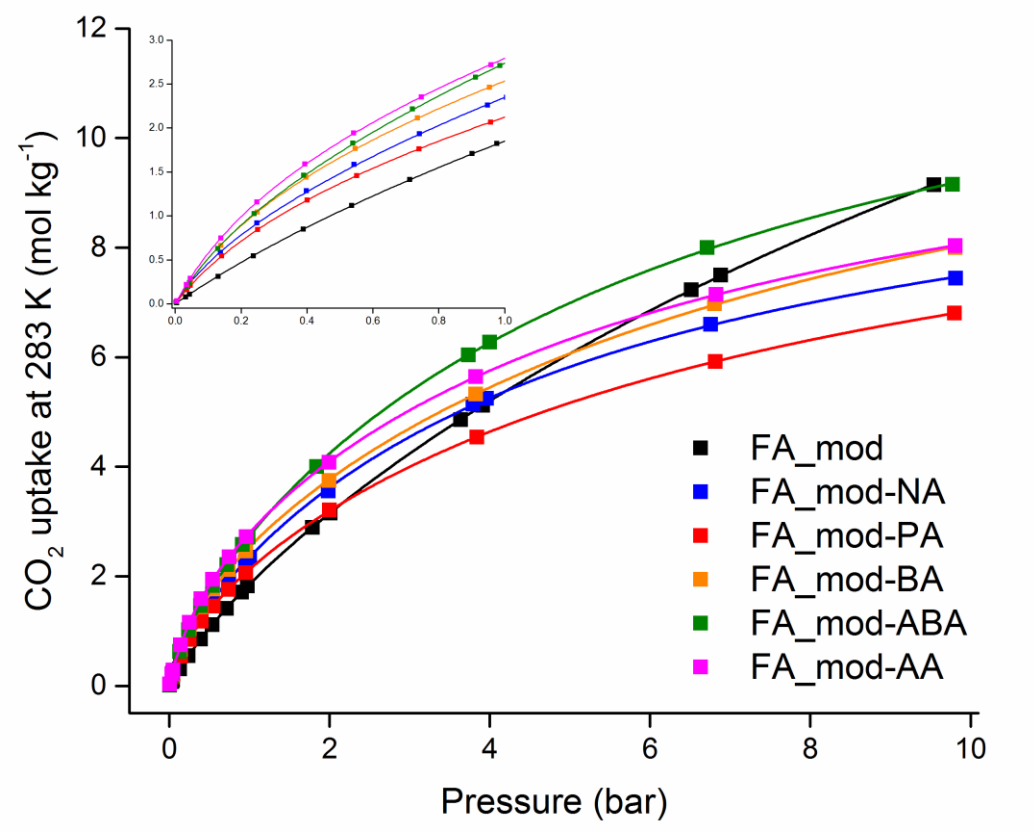

Figure S25. CO_2 excess adsorption isotherms at 283 K of the defective materials

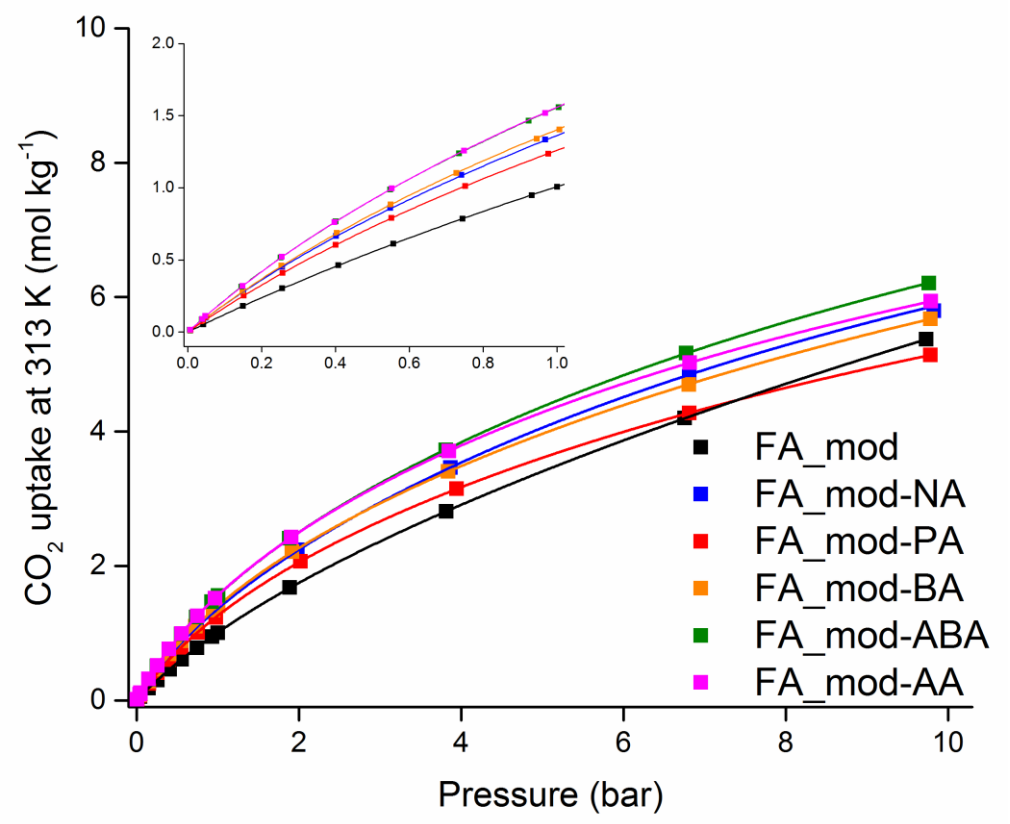

Figure S26. CO_2 excess adsorption isotherms at 313 K of the defective materials

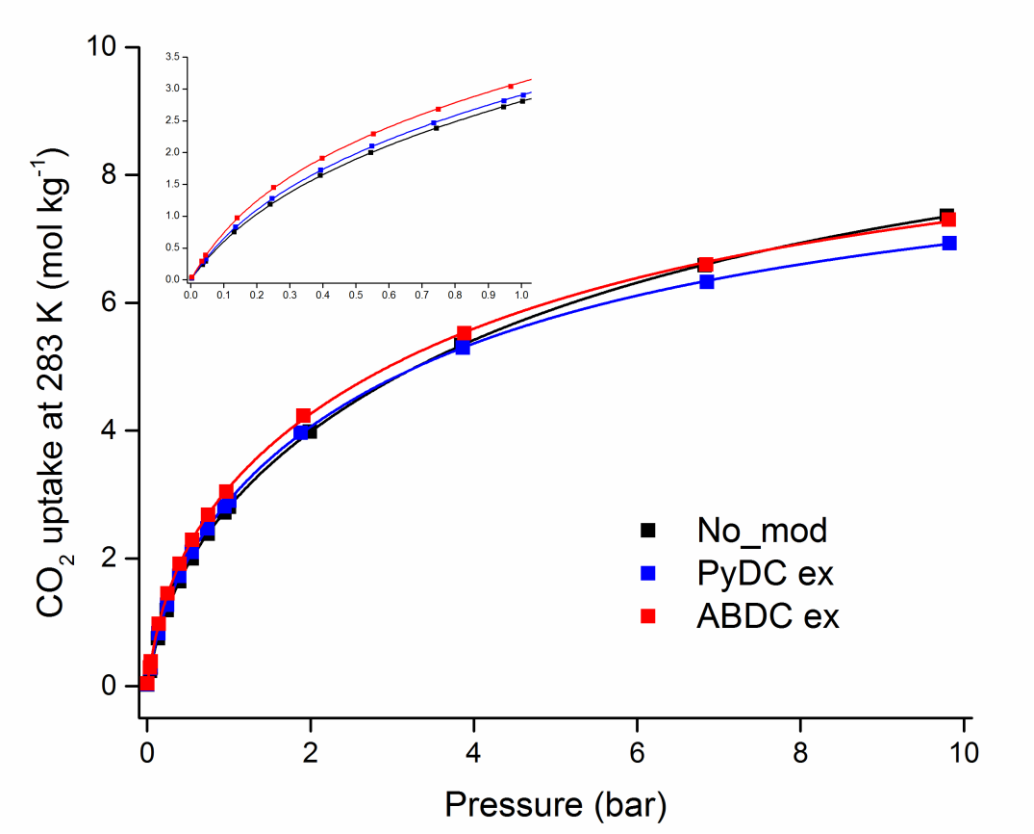

Figure S27. CO_2 excess adsorption isotherms at 283 K of the non- defective materials

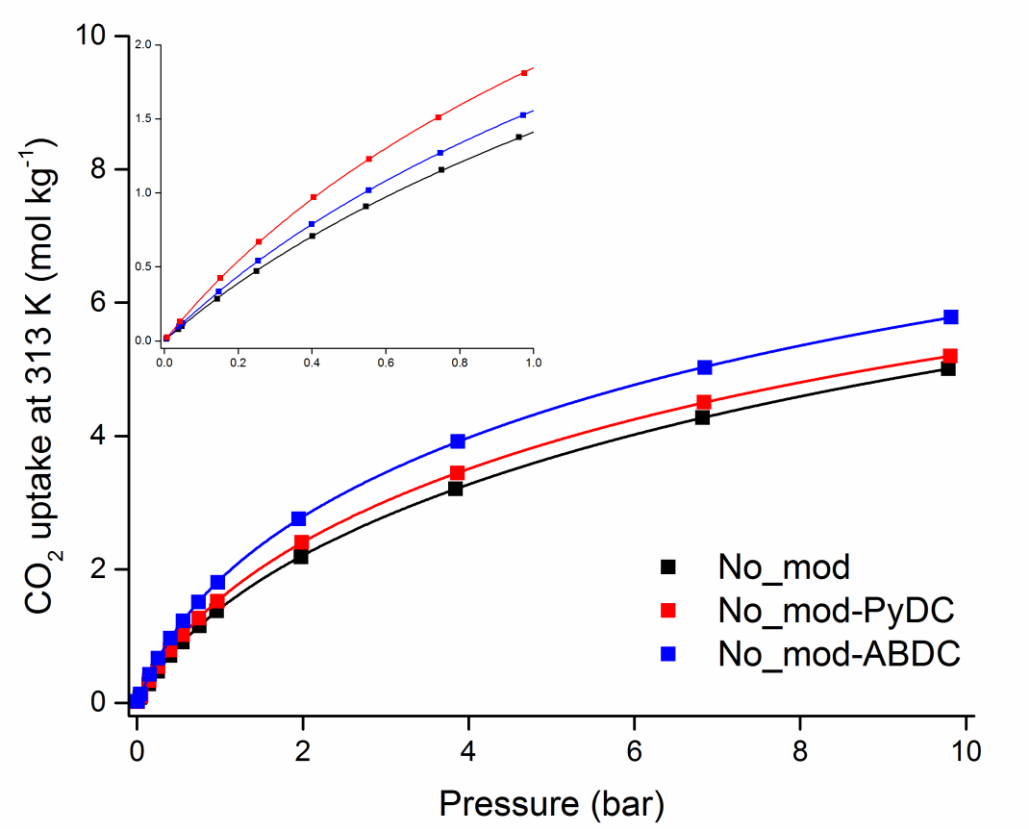

Figure S28. CO_2 excess adsorption isotherms at 313 K of the non- defective materials

Ideal Adsorbed Solution Theory

The most popular model proposed for extracting gas co-adsorption and adsorption selectivity from single-gas isotherms is the Ideal Adsorbed Solution Theory (IAST). Adsorbates are considered to behave as ideal solutions in equilibrium with the gas phase.[2] CO_2 and N_2 single-component adsorption isotherms measured at 298 K and then fitted using suitable adsorption equations. Molar fraction of each species in the adsorbed phase is calculated by solving equation 3:

$$\int_{t=0}^{\frac{P y_1}{x_1}} F_1(t) d \ln t = \int_{t=0}^{\frac{P y_2}{x_2}} F_2(t) d \ln t \qquad (3)$$

where t is a dummy variable, x_i is the molar fraction of component i in adsorbed phase, y_i is the molar fraction of component i in gas phase, F_i is adsorption isotherm function for pure component, and P is the total pressure.

Selectivity is defined as $\frac{\frac{x_1}{y_1}}{\frac{x_2}{y_2}}$

The model was implemented by IAST^{++} software.

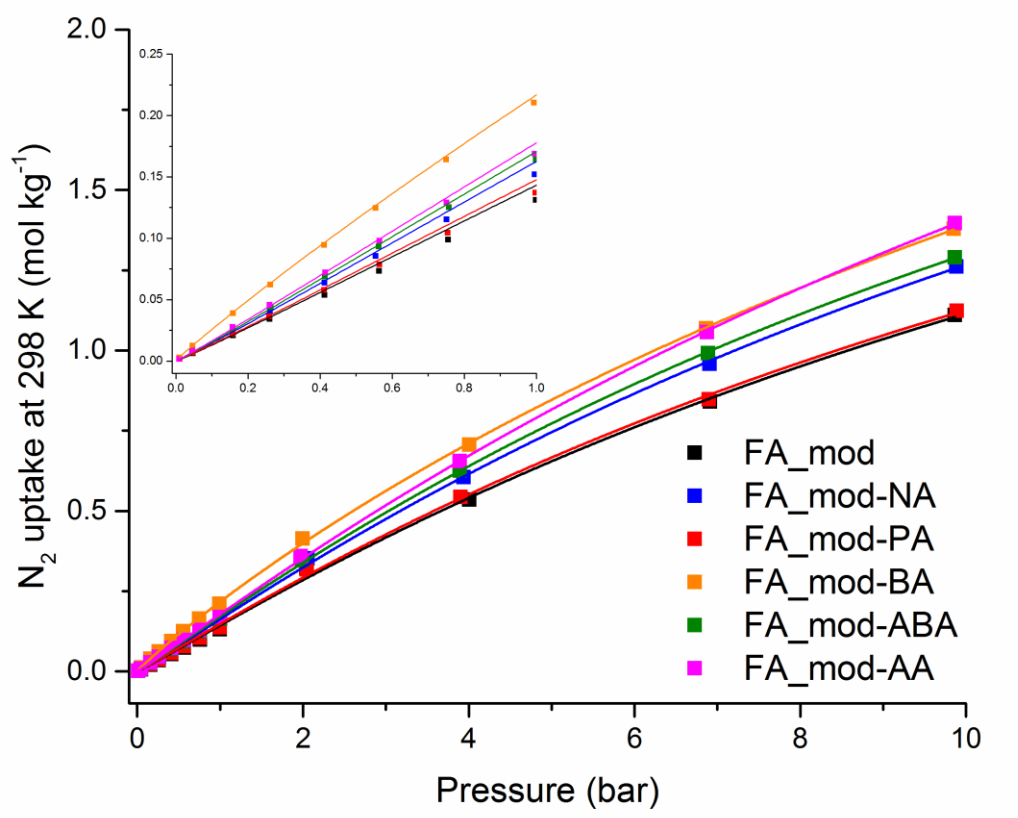

Figure S29. N_2 excess adsorption isotherms at 298 K of the defective materials

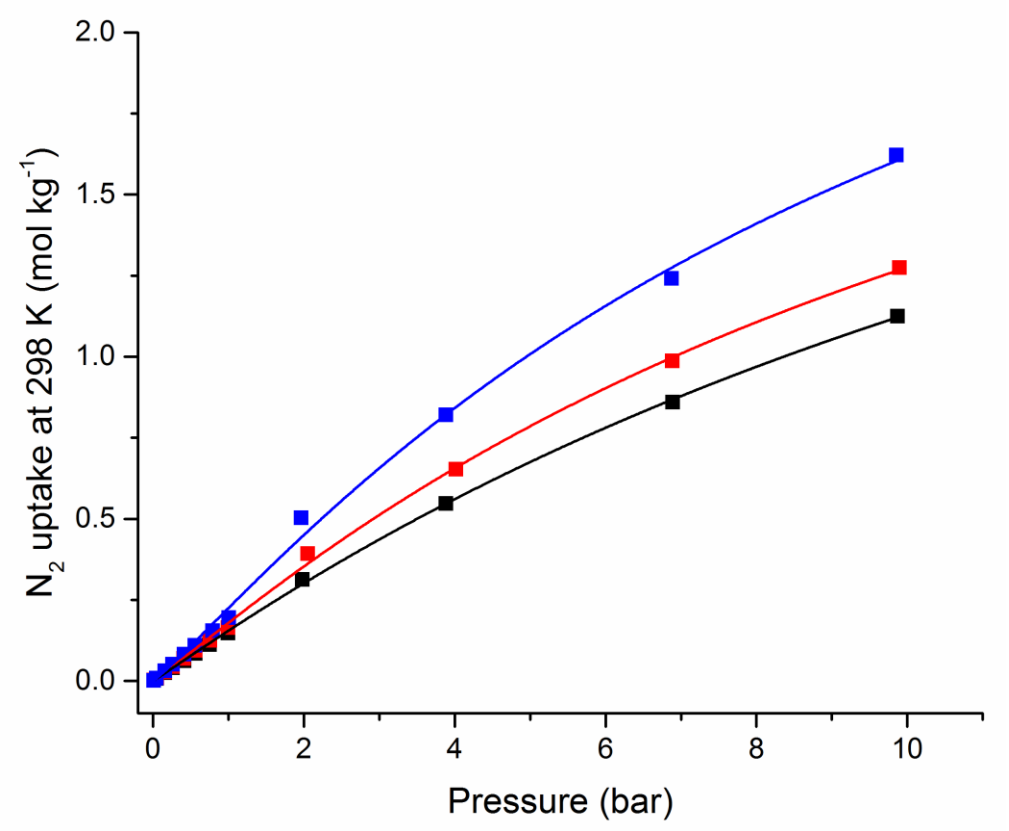

Figure S30. N_2 excess adsorption isotherms at 298 K of the non-defective materials

REFERENCES

1. Park, H. J.; Suh, M. P., Enhanced isosteric heat, selectivity, and uptake capacity of CO2 adsorption in a metal-organic framework by impregnated metal ions. *Chem. Sci.* **2013,** *4* (2), 685-690.
2. Sing, K. S. W.; Rouquerol, F.; Rouquerol, J., 5 - Classical Interpretation of Physisorption Isotherms at the Gas–Solid Interface. In *Adsorption by Powders and Porous Solids (Second Edition)*, Rouquerol, F.; Rouquerol, J.; Sing, K. S. W.; Llewellyn, P.; Maurin, G., Eds. Academic Press: Oxford, 2014; pp 159-189.